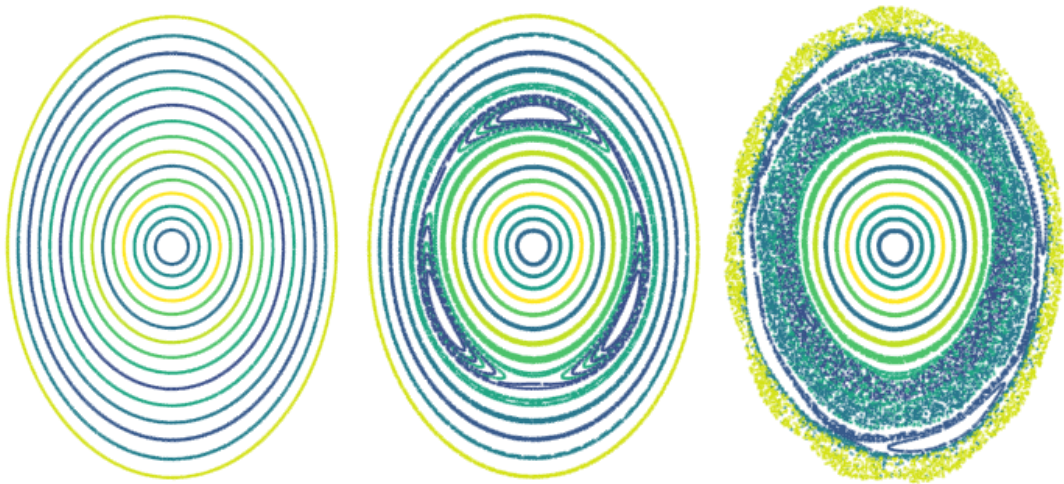# CHALMERS
UNIVERSITY OF TECHNOLOGY

Effects of magnetic perturbations and radiation on the runaway avalanche

Master's thesis in Physics and Astronomy

PONTUS SVENSSON

Effects of magnetic perturbations and radiation on the runaway avalanche

PONTUS SVENSSON

Effects of magnetic perturbations and radiation on the runaway avalanche
Pontus Svensson

Cover: Poincaré plot of the magnetic field structure in an elongated plasma. Three stages of perturbations are shown, complete flux surfaces (left), magnetic islands (centre) and a stochastic edge (right). The figure is obtained by following a field line around a torus, and for every toroidal turn the intersection of the field line with a poloidal plane is marked.

Effects of magnetic perturbations and radiation on the runaway avalanche
PONTUS SVENSSON
Department of Physics
Chalmers University of Technology

Abstract

Electron runaway is seen as one of the main threats to reliable operation of magnetic confinement fusion reactors, and is an issue only predicted to worsen as reactors are scaled up. The runaway phenomenon depends fundamentally on momentum space dynamics, but to simulate large scale systems effective theories which depend only on spatial quantities are often employed. In this thesis, we will address how a momentum space dependent diffusive transport, which appears as a consequence of imperfect confining magnetic fields, can be incorporated into this type of model. A scheme to correct the generation of runaway electrons due to this transport, which incorporates the effect of radiation reaction forces, is proposed. The corrected generation of runaway electrons is formulated as a solution to an integral equation, for which a numerical solver is implemented. The effect of the model is investigated for diffusion coefficients inspired by electron diffusion in stochastic magnetic fields where a reduced generation and a larger critical electric field for the runaway generation is observed.

Acknowledgements

Contents

1

Introduction

Plasmas are abundant in our universe, existing across orders of magnitude in temperature and density. As much as 99% of all matter in the visible universe is estimated to be in the plasma state [1], but here on earth it is relatively rare as a result of the low temperature. Despite this, plasmas play a crucial role on earth, in natural phenomena such as lightning [2] and auroras [3], as well as in man-made contexts such as fluorescent lamps [4], laser-matter interactions [5] and attempts to achieve controlled fusion [6].

A plasma is an ionised gas, which means it is a combination of negatively charged electrons and positively charged ions. However, electrostatic forces prevent a build-up of a net electric charge on large scales, that is the plasma is quasi-neutral, but the small-scale dynamics is nevertheless dominated by the Coulomb interaction. The Coulomb potential decays on a longer length scale than the corresponding potential for neutral atoms [7]. Consequently, the dynamics of plasmas are dominated by grazing collisions, or small angle collisions, in which the particles only change their momentum by a small fraction. This grants plasmas different properties from neutral gases, the dynamics of which are dominated by large angle collisions. One of these is the electron runaway phenomena. Contrary to gases [8], the friction force between particles in a plasma is not monotonically increasing with velocity, but rather has a maximum above which the friction force decreases [9, 10]. Hence if an external force is applied to the plasma, the light electrons which experience a net acceleration will gain energy, and so feel an even smaller friction. This results in a continuous acceleration to relativistic energies, so-called "runaway", until the emission of electromagnetic radiation will act to limit the particle energies [11, 12].

Most investigations of the runaway dynamics have been focused on their generation, but here we will focus on how these energetic particles are transported in a stochastic magnetic field. As a charged particle gyrates around a magnetic field line, the electrons follow the magnetic field line on a large scale. Thus, in a stochastic magnetic field the trajectories of runaway electrons generated close to one another will diverge [13]. This spread is energy dependent and a simplified theory to account for this transport was proposed by Helander et al. [14]. In this thesis we will build on this framework to account for reaction forces caused by radiation from the light emitted from the electrons and investigate the effect of different transport models on the electron runaway.

1.1 Magnetic confinement fusion and tokamaks

In a fusion process two nuclei, small compared to ^{56}Fe, combine and release energy previously stored as binding energy of the nuclei. As a means of generating energy, fusion promises a large scale production, where the main process does not produce greenhouse gases or long-lived radioactive waste, from materials which are plentiful here on earth. In deuterium-deuterium fusion 100 000 kWh of energy is released for every gram fused. Every ton of sea water contains 33g of deuterium making this an essentially unlimited energy resource [15].

Fusion occurs in the collisions between two nuclei. Classically the kinetic energy of the particles must exceed the Coulomb barrier between them; i.e. for two isotopes of hydrogen with charge $-e$,

$$E_k > \frac{e^2}{4\pi\varepsilon_0 r} \sim \text{few MeV}, \tag{1.1}$$

where $r \sim 10^{-15}$m is the radius of the nucleus and ε_0 is the permittivity of free space. However, quantum mechanical tunnelling results in resonance [16, 17] and the fusion reaction between two deuterium nuclei will occur at temperatures of approximately 10 keV[1] [6] which is of the order of hundred millions of degrees. At these temperatures, the hydrogen isotopes are in a plasma state.

Thus the question arises how the plasma should be confined to achieve desired densities and reaction rates to sustain a hot enough plasma for a prolonged time. The most common method in the universe, employed by stars, is to confine the plasma in a gravitational well [18], but this method is not applicable here on earth. An alternative approach is Magnetic Confinement Fusion (MCF) where one confines the fusion plasma with the help of magnetic fields. A charged particle with mass m and charge q, travelling in a constant magnetic field B, will trace out a helix around the magnetic field line as a reaction to the Lorentz force. The radius of this trajectory is the *Larmor radius*,

$$r_L = \frac{mv_\perp}{|qB|}, \tag{1.2}$$

where $v_\perp$ is the velocity of the particle orthogonal to the magnetic field line. Therefore the particle does not have an average velocity perpendicular to the field line and is confined in these two directions, but still behaves like a free particle along the field lines. A natural solution to prevent particles from escaping is to close the magnetic field line in a torus. Two major design types based on this idea exist, the stellarator [19] and the tokamak [6]. The tokamak has a toroidal symmetry but the magnetic geometry of a stellarator is in general more complicated.

We will focus on the tokamak as only this reactor concept has a significant electron runaway problem, due to its use of a toroidal plasma current to produce part of

---

[1]Following plasma physics convention we suppress the Boltzmann constant and describe temperatures in terms of thermal energy.

the magnetic field confining the plasma. The magnetic geometry of a tokamak and coordinates on the torus are shown in figure 1.1a. The toroidal magnetic field in a tokamak B_ϕ is roughly inversely proportional to the major radius of the torus, $B_\phi \sim 1/R$, resulting in a weaker magnetic field on the outside of the torus compared to the inside [6]. The gradient of the magnetic field makes the motion of the particles deviate from the pure Larmor motion and a vertical drift velocity is introduced [20]

$$\boldsymbol{v}_D = \frac{mv_\perp^2}{2Bq}\frac{\boldsymbol{B} \times \boldsymbol{\nabla} B}{B^2}. \tag{1.3}$$

This can be understood as an effect of the Larmor radius being smaller on the high field side compared to the weak field side, the process is schematically described in figure 1.1b[2]. As a consequence of the appearance of the charge q in the drift velocity, which is an effect of the asymmetry of the rotation direction of figure 1.1b, ions and electrons will drift apart, creating a vertical electrostatic field. The electrostatic force qE on the particle will inhibit the gyro motion on half the Larmor orbit and aid it on the other half resulting in a drift towards the low field-side for both ions and electrons. The ions and electrons both drift outwards as the charge dependence of the force cancels the effect of the orientation of gyration. The resulting drift is called the $\boldsymbol{E} \times \boldsymbol{B}$-drift and the drift velocity is [20]

$$\boldsymbol{v}_{\boldsymbol{E} \times \boldsymbol{B}} = \frac{\boldsymbol{E} \times \boldsymbol{B}}{B^2}. \tag{1.4}$$

To stabilise the plasma against these drifts, a poloidal magnetic field is induced by driving a toroidal current in the plasma, the *plasma current*, I_p. The combined magnetic field lines have a helical structure around the torus, allowing the drift on the low and high field side of the tokamak to average out.

1.2 Disruptions and runaway generation

In a tokamak, so-called disruptions can occur, which are violent events where the plasma loses a major part of its thermal energy to the wall; a plasma with a pre-disruption temperature of tens of keV may cool down to just a few eV in a few milliseconds [21]. This has dramatic implications on the electric conductivity of the plasma, which scales as $T^{3/2}$, where T is the plasma temperature [22]. Lenz and Ohm's law combined then means that the electric field driving the plasma current will rise dramatically during a disruption to maintain the current - an electric field which may generate runaway electrons. This is ultimately why stellarators do not have large amounts of runaway electrons, as they do not rely on a plasma current to generate the poloidal component of the magnetic field, but rather use external magnetic field coils - with the expense of a very complicated manufacturing process.

During a disruption in a tokamak the runaway electrons can form a beam in the plasma. If the control of this beam is lost it will hit the inner wall of the machine and cause considerable damage to the plasma-facing components as a large

---

[2]One should note that the so-called curvature drift also introduces a vertical drift which is proportional to the square of the particle velocity along the field line.
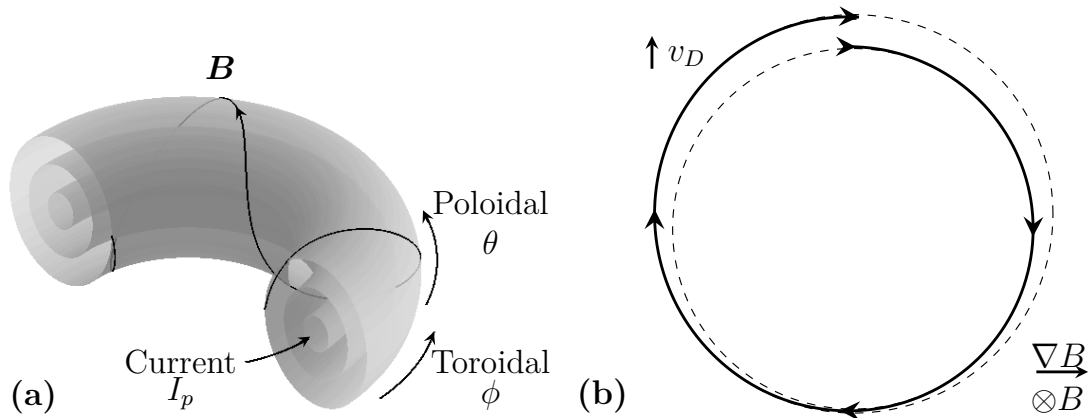
Figure 1.1: (a) Geometry and standard coordinates of a tokamak. Surfaces of constant pressure in the plasma are shown together with a typical magnetic field line. (b) Schematic representation of vertical drifts due to gradient in the magnetic field. Solid line is the particle motion and the dashed circles are the Larmor orbits on the low and high field side.

fraction of the plasma energy content can then be deposited into a small surface area. Significant damage to the inner wall will of course lead to closure of the power plant for repair. The danger of runaway electrons is greatly enhanced by knock-on collisions between the runaway electrons and the thermal population of electrons. After these collisions both runaway and bulk electron may have large enough energy to run away, producing what is called an avalanche, where the runaway electrons exponentially increase in number [23].

Runaways have been extensively studied on existing tokamaks, both in disruptions and generated during steady state operation to assess their properties in detail. Following the initial phase of the disruption where the temperature drops - the thermal quench - the ohmic current and the corresponding electric field dissipates while the runaway electrons are formed - the current quench. When a runaway current is formed, the last phase of the disruption - the runaway plateau - is reached where the entire plasma current is carried by runaway electrons. The beam can be sustained for a long time, as only a small electric field is sufficient to drive the current [24]. Disruptions are also associated with large thermal loads on plasma facing components and structural stress of the vacuum vessel surrounding the plasma. To distribute the thermal load impurities, such as argon and neon, are often released into the plasma, either as a gas or frozen pellets, to radiate thermal energy through line radiation[3] [25]. Impurities with high charge number raise the collisional friction experienced by the runaway electrons, which in principle should be able to reduce their formation. However, a recent study suggests that impurity injection actually increases the runaway generation, as a result of the increased number of target electrons for the avalanche process [26].

---

[3]Originating from excitations of bound electron states.

The largest tokamak to date, ITER [27], is currently under construction in France and it is ongoing work to design the disruption mitigation system for the machine. Electron runaway is seen as one of the main threats to ITER's success, as the number of e-foldings in the avalanche increase drastically when a tokamak is scaled up to ITER parameters from the ones under operation currently. This calls for accurate models for the runaway generation and losses to ensure the design of a successful disruption mitigation system [24, 28].

1.3 Outline

A description of the plasma resolved both kinetically, needed for the runaway problem, and spatially, needed to describe the plasma evolution, becomes unfeasible both analytically and numerically. To describe the evolution of the disruption, simplified fluid models for the runaway populations are often considered [29]. In these, the momentum space dynamics has been captured approximately, and an effective theory only dependent on spatial quantities is used to describe the growth and loss of the runaway population. The goal of this thesis is to present such a theory, describing an effective rate of generation for runaway electrons which incorporates the effects of a momentum space dependent spatial diffusion. The diffusion considered here would originate from the motion of electrons in partially or fully perturbed magnetic fields, which occur naturally after a disruption or may be induced by external magnetic coils. These effective rates of generation can then be used in larger scale disruption simulations to describe the transport of the runaway electrons.

The structure of this thesis is as follows. Chapter 2 explains the underlying theory of the runaway generation, as well as the origin of the spatial diffusion. In chapter 3, we present how the diffusion is incorporated into the fluid description of runaways and the effect it has on the generation of runaway electrons. In chapter 4, we will take a step back and and look at how the correction to the growth rate is calculated for an arbitrary diffusion coefficient, as this process in practice relies on a numerical algorithm. To begin to incorporate gradients of the electric field into the theory, chapter 5 presents a perturbation treatment of the problem, which results in a formulation of the problem of the same structure as that obtained in chapter 3. This allows the problem to again be treated with the numerical methods presented in chapter 4. The validity of this perturbation approach is investigated in chapter 5. Finally, the conclusion in chapter 6 summarises the key points of the thesis.

2

Electron runaway and perturbed magnetic fields

The theoretical background required to follow this thesis is provided in the following chapter. Firstly, a general introduction to plasmas and how to describe electron runaway is presented. This is followed by a description of the motion of a particle in a magnetic field with perturbed field lines, which is the source of the spatial diffusion whose effect on runaways is the focus of this thesis.

2.1 Plasma theory

Plasmas are colloquially known as the the fourth state of matter, after solid, liquid and gas. As the individual constituents of the plasma are charged particles, it acquires unique properties which are used to define it [20]:

> *A plasma is a quasi-neutral gas consisting of charged and neutral particles exhibiting collective behaviour.*

Quasi-neutrality is the property that despite the fact that a plasma consists of individually charged particles, on a large scale the plasma relaxes to a state where there is no net charge density, i.e $\rho = \sum_a q_a n_a \approx 0$, where the index a runs over all the species in the system with charge q_a and density n_a. Large scale in this context is compared to the *Debye length*, which for a plasma of temperature T is $\lambda_D = \sqrt{\varepsilon_0 T / n_e e^2}$. The Debye length is the length scale on which the electric field is exponentially suppressed by screening from the other charges in the system. Concretely the electrostatic potential from a charge q in a plasma where the electrons have had time to relax is [30]

$$\phi(r) = \frac{q}{4\pi\varepsilon_0 r} e^{-r/\lambda_D}. \tag{2.1}$$

For this collective screening to occur, the number of particles within a *Debye sphere*, a sphere with radius λ_D, should be large, $4\pi n_e \lambda_D^3 / 3 \gg 1$.

A detailed microscopic description of a plasma consisting of N-particles would require following the evolution of the system in the $6N$-dimensional phase space, and coupling the dynamics with the electric and magnetic fields through Maxwell's equations. Almost by definition a plasma consists of many particles, making such a detailed description unfeasible both for analytical and numerical progress. Instead

we will work in a statistical description, where the phase space density of particles is the object of consideration. The equation of motion for such an object is the focus of the rest of this chapter.

2.1.1 Kinetic and fluid description

To describe a plasma we use the distribution function $f_a(t, \boldsymbol{x}, \boldsymbol{p})$ of a species a, which is the phase space density of the particles at time t, position $\boldsymbol{x}$ with momentum $\boldsymbol{p}$, normalised such that the spatial density of particles is $n_a(t, \boldsymbol{x}) = \int d^3\boldsymbol{p}\ f_a(t, \boldsymbol{x}, \boldsymbol{p})$. To conserve particle number, particles can only be lost from a phase space volume through its boundary, resulting in continuity equations [31],

$$\frac{df_a}{dt} = \frac{\partial f_a}{\partial t} + \boldsymbol{v} \cdot \frac{\partial f_a}{\partial \boldsymbol{x}} + q_a \left(\boldsymbol{E} + \boldsymbol{v} \times \boldsymbol{B}\right) \cdot \frac{\partial f_a}{\partial \boldsymbol{p}} = 0 \qquad (2.2)$$

which allow for particle acceleration by an electric field $\boldsymbol{E}$ and magnetic field $\boldsymbol{B}$ due to the Lorentz force. The particle velocity $\boldsymbol{v}$ is related to the momentum coordinate by $\boldsymbol{p} = m_a\boldsymbol{v}/\sqrt{1 - v^2/c^2}$ and c is the speed of light. The electric and magnetic fields depend on the distribution function through the Maxwell equations, as the charge ρ and current $\boldsymbol{j}$ densities are related to the distribution function by

$$\begin{aligned} \rho(t, \boldsymbol{x}) &= \sum_a q_a \int d^3\boldsymbol{p}\ f_a(t, \boldsymbol{x}, \boldsymbol{p}) \\ \boldsymbol{j}(t, \boldsymbol{x}) &= \sum_a q_a \int d^3\boldsymbol{p}\ \boldsymbol{v} f_a(t, \boldsymbol{x}, \boldsymbol{p}). \end{aligned} \qquad (2.3)$$

In the absence of collisions equation (2.2) is called the *Vlasov equation.* Then $\boldsymbol{E}$ and $\boldsymbol{B}$ should be seen as large scale electric fields and not as rapidly fluctuating on the microscopic scale. To incorporate the effects of collisions, the Vlasov equation is modified by adding a *collision operator $C\{f_a\}$* on the right hand side of the equation [32] - we will return to this in the following section. The equation describing the evolution of f_a is commonly referred to as the kinetic equation.

The charge and current density are examples of what are called fluid quantities - the momentum space dependence has been integrated out. When the evolution of a system can be cast in terms of fluid quantities, instead of following the full distribution function, the computational cost is significantly lower, and such models can often be used to simulate large scale system evolution. The moments of the kinetic equation result in a coupled set of differential equations for the fluid quantities, one set for each species. In table 2.1 some of the lower velocity moments of the distribution function are shown, and in general all fluid quantities can be derived from the distribution function.

A further reduction often used to study the evolution of the magnetic field is obtained by combining the evolution equations for a given moment of each fluid into a single one. In this *magnetohydrodynamic* (MHD) description [33], centre of mass quantities of the fluids are considered and their coupling to the electromagnetic fields. The

Table 2.1: Lower order fluid moments of the distribution function where $\boldsymbol{w} = \boldsymbol{v} - \boldsymbol{V}$ is the particle random velocity and $\boldsymbol{V}$ is mean flow velocity.

Description	Definition
Density	$n = \int d^3\boldsymbol{p}\, f(t, \boldsymbol{x}, \boldsymbol{p})$
Flow velocity	$\boldsymbol{V} = \frac{1}{n} \int d^3\boldsymbol{p}\, \boldsymbol{v} f(t, \boldsymbol{x}, \boldsymbol{p})$
Temperature	$T = \frac{1}{n} \int d^3\boldsymbol{p}\, \frac{mw^2}{2} f(t, \boldsymbol{x}, \boldsymbol{p})$
Heat flux	$\boldsymbol{q} = \int d^3\boldsymbol{p}\, \boldsymbol{w}\frac{mw^2}{2} f(t, \boldsymbol{x}, \boldsymbol{p})$
Pressure	$\mathbb{P} = \int d^3\boldsymbol{p}\, m\boldsymbol{w}\boldsymbol{w} f(t, \boldsymbol{x}, \boldsymbol{p})$

magnetic equilibrium, for example of a tokamak, follows from the MHD equilibrium equations as

$$\boldsymbol{\nabla} P = \boldsymbol{j} \times \boldsymbol{B} \qquad \text{(Force balance)} \qquad (2.4\text{a})$$

$$\boldsymbol{\nabla} \times \boldsymbol{B} = \mu_0 \boldsymbol{j} \qquad \text{(Ampère's law)} \qquad (2.4\text{b})$$

$$\boldsymbol{\nabla} \cdot \boldsymbol{B} = 0 \qquad \text{(Solenoidality)} \qquad (2.4\text{c})$$

where P is the (isotropic) pressure of the combined fluid [20]. The magnetic field structure in tokamaks will be further discussed in section 2.3.

2.1.2 Collisions and the kinetic equation

A formal treatment of plasma particle collisions can be derived from the Liouville theorem of Hamiltonian dynamics, concluding in the BBGKY hierarchy [34]. Such a formal treatment is not necessary for the work conducted in this thesis and we will be satisfied by a more heuristic approach to introduce the collision operator, which is commonly applied [35]. The Vlasov equation (2.2) describes the conservation of particles if one follows a phase space volume and therefore the collision operator should describe how particles are scattered out of it. If $F(p, \Delta p)$ is the probability that a particle with momentum p will change its momentum by Δp in a time Δt due to collisions, the evolution of the distribution function is

$$f(p, t + \Delta t) = \int d\Delta p\, F(p - \Delta p, \Delta p) f(p - \Delta p, t). \qquad (2.5)$$

In plasmas where small angle collisions dominate, we expand F to second order in Δp, which results in a time evolution, a collision operator, of the form

$$C\{f\} = \left(\frac{\partial f}{\partial t}\right)_{\text{Collisions}} = -\underbrace{\frac{\partial}{\partial p}\left(\frac{\langle \Delta p \rangle}{\Delta t} f\right)}_{\text{Advection}} + \underbrace{\frac{\partial^2}{\partial p^2}\left(\frac{\langle (\Delta p)^2 \rangle}{\Delta t} f\right)}_{\text{Diffusion}} \qquad (2.6)$$

characterised by the first and second Δp moments of the probability distribution F. This is the so-called *Fokker-Planck* collision operator (written for simplicity in one momentum dimension) and takes the form of a combination of advection and a diffusion in momentum space.

We will not present a full derivation of the collision operator here, for such we refer the reader to [35], but rather we will state the results. For non-relativistic electrons, described by a distribution function f, colliding with a species a with charge $Z_a e$, mass m_a and density n_a, which has a Maxwellian velocity distribution of temperature T_a, the resulting collision operator is

$$C_a\{f, f_a\} = \nu_D \mathcal{L}(f) + \frac{1}{v^2}\frac{\partial}{\partial v}v^3\left(\frac{m_e}{m_e + m_a}\nu_s f + \frac{1}{2}\nu_{\|}v\frac{\partial f}{\partial v}\right) \tag{2.7}$$

and the combined effect of collisions with multiple species is obtained by summing the contribution from the individual species, $C\{f\} = \sum_a C_a\{f, f_a\}$. The frequencies in the collision operator are defined as

$$\nu_D = \hat{\nu}_{ea}\frac{\operatorname{erf}(v/v_{Ta}) - \mathcal{G}(v/v_{Ta})}{(v/v_{Te})^3} \qquad \text{(Deflection frequency)} \tag{2.8a}$$

$$\nu_s = \hat{\nu}_{ea}\frac{2T_e}{T_a}\left(1 + \frac{m_a}{m_e}\right)\frac{\mathcal{G}(v/v_{Ta})}{v/v_{Te}} \qquad \text{(Slowing-down frequency)} \tag{2.8b}$$

$$\nu_{\|} = 2\hat{\nu}_{ea}\frac{\mathcal{G}(v/v_{Ta})}{v/v_{Te}} \qquad \text{(Parallel diffusion frequency)} \tag{2.8c}$$

$$\hat{\nu}_{ea} = Z_a^2\frac{n_a e^4 \ln\Lambda}{4\pi\varepsilon_0^2 m_e^2 v_{Te}^3} \qquad \text{(Thermal collision frequency)} \tag{2.8d}$$

where v_{Ta} and v_{Te} are the thermal velocities of a and the electrons[1], $v_{Ta} = \sqrt{2T_a/m_a}$ and $\ln\Lambda = \ln(4\pi\lambda_D^3 n_e)$ is the Coulomb logarithm, which characterises the effect of a screened electric field on longer distances then λ_D. Typical values for the Coulomb logarithm for fusion plasmas are in the range of $10 - 20$. The function $\mathcal{G}(x) \equiv \frac{\operatorname{erf}(x) - x\operatorname{erf}'(x)}{2x^2}$ is the *Chandrasekhar function*[2] and the operator $\mathcal{L}$ is the Lorentz scattering operator

$$\mathcal{L} = \frac{1}{2}\frac{\partial}{\partial \xi}\left(1 - \xi^2\right)\frac{\partial}{\partial \xi} + \frac{1}{2}\frac{1}{1 - \xi^2}\frac{\partial^2}{\partial \varphi^2} \tag{2.9}$$

which describes diffusion on a sphere of constant p in momentum space. When discussing dynamics in a magnetic field one often introduces a spherical coordinate system for the momentum (p, ξ, φ) where the "z-axis" is aligned with the magnetic field. The magnitude of the momentum is p, the cosine of the polar angle, also known as the pitch angle[3], is $\xi = \cos\theta = p_{\|}/p$ and φ is the azimuthal angle or gyro angle. From now on all quantities with the subscript $\|$ are components along the magnetic field line and those with $\perp$ are perpendicular to it. Note that, when there is no parameter variation on scales shorter than the gyroradius, we can often simply average over the gyro angle dependence of the kinetic equation, as it will just describe the gyration around the magnetic field line.

---

[1]It is not necessary to introduce an electron temperature T_e as it cancels and the electron does not need to be in thermal equilibrium.

[2]The function $\operatorname{erf}(x)$ is the error function defined as $\operatorname{erf}(x) = \frac{2}{\pi}\int_0^x e^{-y^2}dy$.

[3]Here θ is not to be confused with the poloidal angle in a tokamak, defined in figure 1.1a.
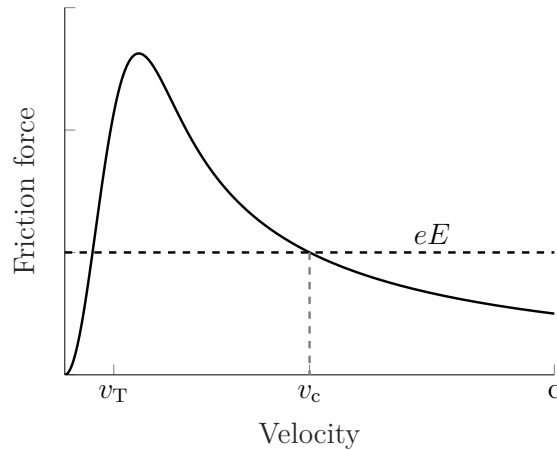
Figure 2.1: Illustration of the friction force in plasma as a function of electron velocity. The friction force has a maximum close to the thermal velocity v_{Te} and is a decreasing function with high velocities at large energies. If an electric field E is applied to the plasma along the magnetic field line, electrons with a larger velocity than v_c will experience a net acceleration and run away.

The effective friction in the system follows from equation (2.7), proportional to $v\nu_s \propto \mathscr{G}\left(v/v_{Ta}\right) \to 0.5\; v_{Ta}^2/v^2$ when $v \gg v_{Ta}$. This is the origin of the electron runaway, as the friction force decreases at higher velocities as shown in figure 2.1. The momentum at which an electric field along the magnetic field line balances the friction is called the critical momentum p_c, above which electrons run away. The Dreicer field [36, 37],

$$E_D = \frac{n_e e^3 \ln \Lambda}{4\pi\varepsilon_0^2 T_e} \tag{2.10}$$

sets the scale at which the electric field overcomes the internal friction, and all of the population will run away, slide-away, when the electric field exceeds $\max_x\{\mathscr{G}(x)E_D\} \approx 0.2E_D$ [38].

For the runaway electrons we need a relativistic collision operator due to their large energy - comparatively all other particles can be seen as stationary, $T_e \ll m_e c^2$. Using a momentum coordinate p which is normalised to $m_e c$ such that the γ-factor is $\gamma = \sqrt{1 + p^2}$, the collision operator takes the form [35]

$$C\{f\} = \nu_D \mathscr{L}(f) + \frac{1}{p^2}\frac{\partial}{\partial p}\left(p^3 \nu_s f\right), \tag{2.11}$$

where ν_s is dominated by electron-electron collisions but ν_D has significant contributions from both the electrons and ions in the plasma. The characteristic time scale in the problem is now the relativistic collision time between electrons $\tau = 4\pi\varepsilon_0^2 m_e^2 c^3 / n_e e^4 \ln \Lambda_c$, where $\ln \Lambda_c$ is the relativistic Coulomb logarithm, $\ln \Lambda_c = \ln \Lambda + 0.5 \ln\left(m_e c^2/T\right)$. The relativistic generalisations for ν_s and ν_D are, in units of τ^{-1},

$$\nu_D = \frac{\gamma}{p^3}\bar{\nu}_D$$
$$\nu_s = \frac{\gamma^2}{p^3}\bar{\nu}_s \qquad (2.12)$$

where for the case of fully ionised ions $\bar{\nu}_s = 1$ and $\bar{\nu}_D = 1 + Z_{\text{eff}}$ [39]. As already could be noted from equation (2.8a), the deflection coefficient is not dependent on the ion mass but just the square of its charge, and therefore multiple ion species act as a single ion species with an effective charge $Z_{\text{eff}} = \sum_a \frac{n_a}{n_e} Z_a^2$. The parallel diffusion in momentum space is a consequence of the finite thermal speed, which is neglected in the super-thermal limit, $v \gg v_{Te}$.

Whereas the friction in the non-relativistic case tends to zero for large velocities, the friction force for the relativistic collision operator (2.11) saturates as $\gamma \to \infty$ to $m_e c\bar{\nu}_s$, which sets a lower limit for the required electric field along a magnetic field line to generate runaway electrons. This lower limit in a fully ionised plasma is called the critical electric field [40]

$$E_c = \frac{m_e c}{e\tau} \approx \frac{T}{m_e c^2} E_D. \qquad (2.13)$$

The two electric fields, E_D and E_c, concern different energy scales, the thermal and relativistic scales, and govern two different aspects of the runaway problem, primary and secondary generation, which will be described further on in section 2.2.

Some recent developments have incorporated the effects of partially ionised ions in the plasma, which result in a screening of the full charge of the nucleus. The screening acts differently depending on the energy scale, as a relativistic electron may penetrate the cloud of bound electrons and "feel" a larger charge compared to low energy electrons, which are only influenced by the net charge of the ion. The effects are incorporated by generalising $\bar{\nu}_D$ and $\bar{\nu}_s$ for relativistic electrons to [41, 42]

$$\bar{\nu}_D \approx 1 + Z_{\text{eff}} + \frac{1}{\ln\Lambda_c}\sum_a \frac{n_a}{n_e}\left[\left(Z_a^2 - Z_{0a}^2\right)\ln\bar{a}_a - \frac{2}{3}N_a^2\right] + \frac{\ln p}{\ln\Lambda_c}\sum_a \frac{n_a}{n_e}Z_a^2 \qquad (2.14a)$$

$$\bar{\nu}_s \approx 1 + \frac{1}{\ln\Lambda_c}\sum_a \frac{n_a}{n_e}N_a\left(\ln I_a^{-1} - 1\right) + \frac{\ln p}{2\ln\Lambda_c}\left(1 + 3\sum_a \frac{n_a}{n_e}N_a\right) \qquad (2.14b)$$

or with the notation $\bar{\nu}_D \approx \bar{\nu}_{D0} + \bar{\nu}_{D1}\ln p$ and $\bar{\nu}_s = \bar{\nu}_{s0} + \bar{\nu}_{s1}\ln p$. These collision frequencies now depend on atomic parameters of species a: Z_{0a} ionisation degree, Z_a atomic number, $N_a = Z_a - Z_{0a}$ electron number, I_a mean excitation energy and the effective ion size $\bar{a}_a$ determined from density functional theory (DFT) calculations [41]. The effect of partially ionised ions in the plasma will influence the runaway generation as well as increase the critical electric field.

2.1.3 Radiation reaction forces

An accelerated charge, which an electron circulating around a magnetic field line most definitely is, will emit electromagnetic radiation which itself carries a momentum. A radiation reaction force is thus needed to act on the charge to enforce conservation of total momentum. This force will alter the motion of the particles and must be accounted for in the time evolution of the distribution function by the addition of source terms to the kinetic equation (2.2).

There are two main types of radiation losses to account for, synchrotron radiation and bremsstrahlung. For relativistic particles the head light effect directs this radiation predominantly in the forward direction of the electron orbit [43], resulting in a reaction force. The term in the kinetic equation resulting from this force is [12, 44]

$$\frac{\partial}{\partial \boldsymbol{p}} \cdot (\boldsymbol{F}_{\mathrm{syn}} f) = -\frac{1}{p^2} \frac{\partial}{\partial p} \left(\frac{p^3 \gamma}{\tau_{\mathrm{syn}}} \left(1 - \xi^2 \right) f \right) + \frac{\partial}{\partial \xi} \left(\frac{\xi \left(1 - \xi^2 \right)}{\tau_{\mathrm{syn}} \gamma} f \right) \tag{2.15}$$

where τ_{syn} is the synchrotron radiation-damping time scale, which in units of τ is

$$\tau_{\mathrm{syn}} = \frac{6\pi \varepsilon_0 m_e^3 c^3}{\tau e^4 B^2}. \tag{2.16}$$

The synchrotron radiation primarily has a slowing down effect, which is maximised when $\xi = 0$ i.e. when the electron is just circulating around the field line.

The effects of bremsstrahlung can be treated with the Boltzmann operator, taking the form of an integral operator over the distribution function and the differential cross section for the bremsstrahlung. Based on the simplified form factor presented in Ref. [41], the effects of bremsstrahlung are incorporated into the kinetic equation by the term [45]

$$\frac{\partial}{\partial \boldsymbol{p}} \cdot (\boldsymbol{F}_{\mathrm{br}} f) = -\frac{1}{p^2} \frac{\partial}{\partial p} \left(p^2 F_{\mathrm{br}} f \right) \tag{2.17}$$

where F_{br} is approximated by

$$F_{\mathrm{br}} \approx \frac{p\alpha}{\ln \Lambda_c} \sum_a \frac{n_a}{n_e} Z_a^2 \left(0.35 + 0.20 \ln p \right) \equiv p \left(\phi_{\mathrm{br}0} + \phi_{\mathrm{br}1} \ln p \right) \tag{2.18}$$

and α is the fine structure constant.

Altogether we now have a gyro averaged kinetic equation following from equation (2.2) of the form

$$
\begin{aligned}
\tau \frac{\partial \bar{f}}{\partial t} = {} & \frac{\partial}{\partial p} \left[\left(-\xi E + p\nu_s + F_{\mathrm{br}} + \frac{p\gamma}{\tau_{\mathrm{syn}}} \left(1 - \xi^2 \right) \right) \bar{f} \right] \\
& + \frac{\partial}{\partial \xi} \left[\left(1 - \xi^2 \right) \left(-\frac{E}{p} \bar{f} + \frac{1}{2} \nu_D \frac{\partial \bar{f}}{\partial \xi} \right) - \frac{\xi \left(1 - \xi^2 \right)}{\tau_{\mathrm{syn}} \gamma} \bar{f} \right],
\end{aligned}
\tag{2.19}
$$

where E the electric field along the magnetic field line is normalised to E_c and $\bar{f} = 2\pi p^2 f$ is the distribution function multiplied by the measure in momentum-space after integration over the gyro-angle. This is almost the complete kinetic

equation which we will work with. In section 2.3 we will add the new part, effects of spatial diffusion due to perturbed magnetic fields, but first we will consider the rates of runaway electron generation without influence of spatial diffusion.

2.2 Runaway electron generation

The first person to describe the runaway phenomena was C.T.R. Wilson in the early 20th century, when he analysed β-particles in a strong electrostatic field motivated by his investigation of thunderclouds [46, 47]. But the first to use the term "runaway" was the English astronomer and physicist Eddington, in his *The Internal Constitution of the Stars* from 1926 [48]. Dreicer in 1959 was the first with a more rigorous treatment, when the total friction between two Maxwellian populations was considered [36]. He concluded, for electric fields of the order of E_D, all the electrons would run away towards infinite energies.

Most of the early investigations of runaway electrons considered how momentum space diffusion feeds the runaway region with electrons, from which they run away towards relativistic energies. This process we now call primary or Dreicer generation. Kruskal and Bernstein in 1964 were the first to properly solve the kinetic equation, by finding the solution in five different velocity regions and then asymptotically matching the solutions in these different regions [49]. As well as providing the velocity distribution function, this solution gave the rate of runaway production. However this theory was still not relativistic and arbitrarily small electric fields could generate the runaway. In 1975, Connor and Hastie presented a relativistic generalisation of the calculation, which introduced the critical electric field E_c. The relativistically correct runaway generation rate was found to be [40]

$$\left(\frac{\partial n_{\mathrm{RE}}}{\partial t}\right)_{\mathrm{Primary}} = C \frac{n_e}{\hat{\nu}_{ee}^{-1}} \left(\frac{E}{E_D}\right)^{-\frac{3}{16}(1+Z_{\mathrm{eff}})h} \exp\left[-\lambda\frac{E_D}{4E} - \sqrt{\eta\frac{(1+Z_{\mathrm{eff}})\,E_D}{E}}\right], \quad (2.20)$$

where

$$\begin{aligned}
\lambda &= 8\left(\frac{E}{E_c}\right)^2\left[1 - \frac{1}{2}\frac{E_c}{E} - \sqrt{1 - \frac{E_c}{E}}\right] \\
\eta &= \frac{1}{4}\frac{E^2}{E_c\,(E - E_c)}\left[\frac{\pi}{2} - \arcsin\left(1 - \frac{2E_c}{E}\right)\right]^2 \\
h &= \frac{1}{3}\frac{E_c}{E - E_c}\left[\frac{E}{E_c} + 2\left(\frac{E}{E_c} - 2\right)\sqrt{\frac{E}{E - E_c}} - \frac{Z_{\mathrm{eff}}}{Z_{\mathrm{eff}} + 1}\right]
\end{aligned} \quad (2.21)$$

and C is a undetermined constant of order unity. The dominant scaling in equation (2.20) is $\exp\left(-E_D/4E\right)$, thus the primary generation rate is exponentially sensitive to temperature and the relevant scale for the electric fields is the Dreicer field.

Existing runaway electrons have a tendency to multiply through the avalanche mechanics. This secondary generation is a result of a knock-on collision between a
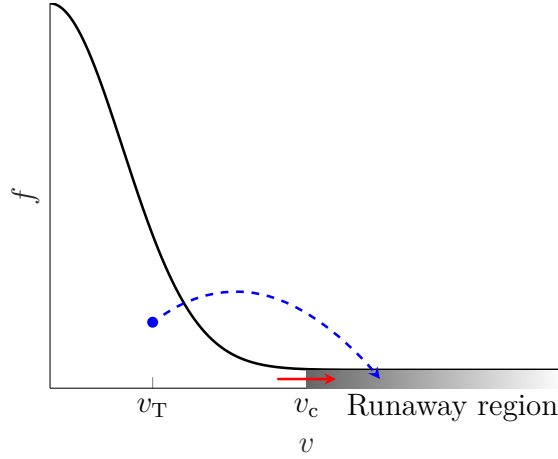
Figure 2.2: Illustration of primary (solid arrow) and secondary (dashed arrow) generation of runaway electrons. Primary generation is a result of momentum space diffusion due to collisions resulting in particles diffusing into the runaway region. Secondary generation occurs in large angle collisions between a thermal electron (a dot in the illustration) and a runaway electron, such that after the collision both the electrons run away.

runaway electron and a thermal one, resulting in both electrons ending up in the runaway region after the collision [50, 51]. In knock-on collisions the trajectory of the runaway electron is not significantly deflected, but the change in momentum space of the thermal electron is characterised by the source term of the avalanche mechanics [23],

$$S_{\text{Ava}} = \frac{n_{\text{RE}}}{\tau \ln \Lambda_c} \delta^{(1)}(\xi - \xi_2) \frac{1}{p^2} \frac{\partial}{\partial p} \left(\frac{1}{1 - \sqrt{1 + p^2}} \right), \tag{2.22}$$

where ξ_2 is the pitch angle of the secondary electron, determined by energy conservation to be $\xi_2 = \sqrt{\frac{\gamma - 1}{\gamma + 1}}$ and here γ is the Lorentz factor. Two main characteristics should be noted. Firstly, the source term is proportional to the current number of runaway electrons n_{RE}, giving rise to the exponential growth of the avalanche. Secondly, the characteristic time scale is significantly longer than the collision time, as it is a factor of $\ln \Lambda$ longer. A solution of the kinetic equation with this source term resulted in a growth rate, interpolated between solutions in several different regions of parameter space, of [23]

$$\begin{aligned} \gamma \equiv \frac{1}{n_{\text{RE}}} \left(\frac{\partial n_{\text{RE}}}{\partial t} \right)_{\text{Ava}} &= \frac{1}{\tau \ln \Lambda} \sqrt{\frac{\pi}{3 \left(Z_{\text{eff}} + 5 \right)}} \left(\frac{E}{E_c} - 1 \right) \\ &\times \left(1 - \frac{E_c}{E} + \frac{4\pi \left(1 + Z_{\text{eff}} \right)^2}{3 \left(Z_{\text{eff}} + 5 \right) \left(E^2/E_c^2 + 3 \right)} \right)^{-\frac{1}{2}}, \end{aligned} \tag{2.23}$$

in the limit of large aspect ratio, where the effect of the toroidal geometry of a tokamak has been neglected. Both the primary and secondary generation is schematically illustrated in figure 2.2.

The avalanche growth is sensitive to the electric field strength and consequently the number of runaways generated depends on the evolution of the electric field after the disruption. The time derivative of Ampère's law, in a source free environment and where the displacement current is neglected, results in an inductive equation for the electric field strength along the magnetic field line [29],

$$\nabla^2 E_{||} = \mu_0 \frac{\partial j_{||}}{\partial t}. \tag{2.24}$$

To perform a zero dimensional analysis of a cylindrical plasma with toroidal and poloidal symmetry, we introduce a characteristic radial length scale Δ, and replace $\nabla^2 E_{||} = -E_{||}/\Delta^2$ as well as $I = 2\pi\Delta^2 j_{||}$, where I is the total current. If the runaway generation is small enough to not significantly impact the electric field evolution, the current is primarily ohmic, $I \approx 2\pi\Delta^2\sigma E_{||}$, with the plasma conductivity σ, resulting in an exponential decay of the electric field strength with a time constant $t_{CQ} = \mu_0\Delta^2\sigma$. For such a time evolution the number of e-foldings for the avalanche, based on a large E approximation of (2.23) is,

$$\int_0^\infty dt\, \gamma \approx \int_0^\infty dt\, \frac{E}{\sqrt{5 + Z_{\text{eff}}}\tau E_c \ln \Lambda} = \frac{2}{\sqrt{5 + Z_{\text{eff}}}}\frac{I_p}{I_A \ln \Lambda}, \tag{2.25}$$

where $I_A = 4\pi m_e c/\mu_0 e \approx 17\text{kA}$ is the Alfvén current. So the number of generated runaway electrons increases with the plasma current I_p in the exponent, predicting a drastic increase as tokamaks are scaled up. It should be noted though that for large tokamaks the effect of runaways cannot be neglected in the electric field evolution, and the runaway current is limited by the plasma current.

Bound electrons and screening effects will influence the avalanche growth rate and developments in the last years have shown that the avalanche growth rate in the presence of partially ionised ions is well described by [26]

$$\gamma = \frac{n_e^{\text{tot}}/n_e}{\tau \ln \Lambda_c} \frac{1}{\sqrt{4 + \bar{\nu}_D(p_\star)\bar{\nu}_s(p_\star)}} \frac{E - E_c^{\text{eff, rad}}}{E_c}, \tag{2.26}$$

where n_e^{tot} is the total density of bound and free electrons and $E_c^{\text{eff, rad}}$ is the new critical electrical field described in Ref. [39]. The momentum $p_\star$ is determined implicitly by the equation

$$p_\star = \frac{\sqrt[4]{\bar{\nu}_D(p_\star)\bar{\nu}_s(p_\star)}}{\sqrt{E/E_c}} \tag{2.27}$$

and acts as an effective critical momentum above which electrons run away.

2.3   Electrons in a perturbed magnetic field

In MCF, the plasma is confined by a magnetic field allowing for a temperature gradient from a hot core to the cold edge of the plasma. For a plasma in equilibrium this is equivalent to a pressure gradient $\boldsymbol{\nabla} P$, and the magnetic structure is therefore determined by the force balance between the pressure and electromagnetic force, described by (2.4a). Accordingly the magnetic field lines must lie on surfaces of constant pressure, as

$$\boldsymbol{B} \cdot \boldsymbol{\nabla} P = 0. \tag{2.28}$$

For such a system to be spatially bounded, the surfaces of constant pressure need to be topologically equivalent to tori [52]. The fundamental magnetic geometry of a tokamak or stellarator is to have such surfaces nested around each other.

In a perturbed magnetic field structure, a so-called magnetic island can be formed, which is a separate pressure surface, isolated from the rest of the plasma, in the shape of a closed tube. When the perturbation grows, the size of the island grows with it and as islands centered on different magnetic surfaces start to overlap, the magnetic field lines become stochastic [53]. A stochastic field is where a single field line comes arbitrarily close to all points in some region [52]. In the following sections, 2.3.1 to 2.3.3, we will discuss the motion of electrons in these stochastic magnetic fields, where the effective radial transport will be described by a diffusive process.

2.3.1   Experimental evidence of runaway transport

Stochastic fields are thought to occur naturally in the early stages of the disruption, as a result of the effects of instabilities which initiate the disruption. Simulations based on the MHD-equations with the JOREK code, have indeed shown largely stochastic magnetic fields in the initial phases of the disruption [54]. However, the flux surfaces can partially or fully heal, which led to the idea of externally influencing the field to enhance the effect.

Resonant Magnetic Perturbation (RMP) is a method to generate perturbations of the magnetic field by the means of external magnetic field coils. During a disruption this is with the intention to increase transport and hinder the avalanche growth of runaway electrons. The method has been tested in smaller tokamaks, JT-60U [55] and TEXTOR [56], and for sufficient perturbation of the magnetic field runaways are absent from the disruption. The required magnitude of the pertubation was found to be on the order of $\delta B / B \sim 10^{-3}$. The hypothesis is that particles are transported out of the machine before they have had time to multiply by the avalanche mechanism.

Investigations with RMPs on the larger JET tokamak, have not had the same success - no significant effects on the runaway generation have been observed [57]. How large the ergodic regions of the magnetic fields were in these experiments could not be determined directly experimentally, but numerical calculations suggest that

there was quite a small overlap between islands, which could be an explanation of the limited effect seen in [57], as large-scale ergodic regions would not be formed. Numerical investigations of the intended ITER RMP system have shown that the runaway electrons in the core would be well confined, but with perturbations of the order $\delta B/B \gtrsim 10^{-3}$ runaway electrons in the outer regions of the plasma will be rapidly lost [58, 59].

2.3.2 Particles following perturbed field lines

The light electrons will in general follow the magnetic field lines as a result of the Lorentz force. Some basic understanding of the transport of particles in a stochastic field can therefore be gained just by following the magnetic field lines. It is such a model for the transport we will consider in this section.

The original treatment of transport resulting from perturbed magnetic field lines was introduced by Rechester and Rosenbluth in a cylindrical geometry [13]. They considered the effect of magnetic perturbations arising due to overlapping magnetic islands. A plasma cylinder of length $2\pi R$ with periodic boundary conditions, was considered to mimic a torus with major radius R. In the cylindrical coordinate system (r, θ, z) the magnetic field takes the form $\boldsymbol{B} = B_\varphi \hat{z} + B_\theta(r)\hat{\theta} + \delta\boldsymbol{B}$, where B_φ and B_θ are the toroidal and poloidal magnetic field components and $\delta\boldsymbol{B}$ is the perturbation. For the boundary condition to be satisfied, the perturbation is expanded in a Fourier series as [13],

$$\delta\boldsymbol{B} = \sum_{m,n} \boldsymbol{b}_{mn}(r)e^{i(m\theta - nz/R)} + \text{c.c.} \tag{2.29}$$

Consider a small area at a constant z_0 which is mapped along the magnetic field line some distance to z_1. This mapping is area preserving, as $\boldsymbol{\nabla} \cdot \boldsymbol{B} = 0$, but the trajectories of the magnetic field lines will generally diverge, resulting in a shape with a large amount of detail, a process commonly known as *magnetic braiding* [13]. An example of this process is shown in figure 2.3. This process in a stochastic magnetic field was shown by Refs. [60, 61] to result in a diffusive process described by the diffusion coefficient

$$D_{\text{st}}(r) \equiv \frac{\langle (\Delta r)^2 \rangle}{2L} = \pi R \sum_{m,n} \frac{|\boldsymbol{b}_{mn}(r)|^2}{B_\varphi^2} \delta^{(1)}\left(\frac{m}{q(r)} - n\right) \tag{2.30}$$

where $\langle (\Delta r)^2 \rangle$ is the mean square displacement of the trajectories and L is the length propagated along z. The safety factor $q(r)$ is the number of toroidal turns a magnetic field line makes for every poloidal turn.

This mapping is fully deterministic and to obtain a physical diffusion coefficient it should be multiplied with a speed along the field line [13]. This transport is fundamentally based on the length propagated along the field line and so this effect saturates as $v \to c$ in the relativistic limit.
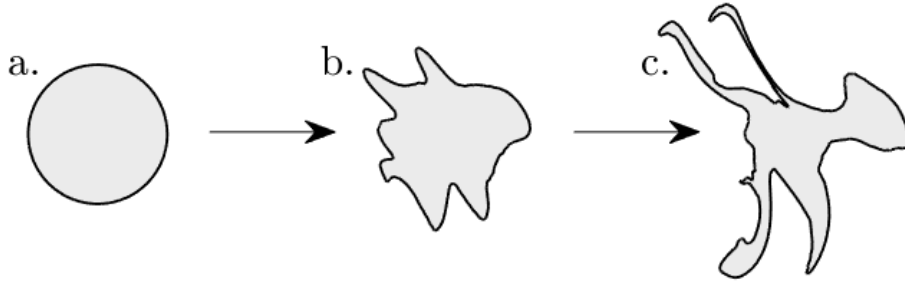
Figure 2.3: Different stages of the magnetic braiding. The initial area in a toroidal plane (a), and how this is mapped along the magnetic field lines to two other toroidal planes, first (b) and then further to (c).

The essence of the treatment above was later generalised to provide a description of radial transport in a perturbed field of arbitrary origin and toroidal geometry [62]. Following the above, the radial velocity of particles following magnetic field lines was considered to be $v_B \simeq v_{||} \, \delta B_r / B$, where δB_r is the root mean square of the radial perturbation of the magnetic field. The correlation time was taken to be due to moving a particle through the poloidal mode structure, $\tau_{||} = \lambda_{||}/v_{||} \simeq \pi q R/v_{||}$, where the parallel connection length $\lambda_{||} \simeq \pi q R$ is taken as a simple approximation to the parallel correlation length. This may be expected to give an overestimate for compact poloidal mode structures, but an additional effect that may be more important is discussed in the next section. In the limit of small *Kubo numbers* [63] (the particle is decorrelated due to its parallel motion and not its radial one) the diffusion coefficient is therefore approximately

$$D(r) = v_B^2 \tau_{||} = \pi q R \left(\frac{\delta B_r(r)}{B} \right)^2 v_{||}, \tag{2.31}$$

which is the low energy dependence of the diffusion coefficients we will investigate in this thesis. In the high energy limit, orbit averaging effects are believed to be important and are discussed in the following section.

2.3.3 Orbit averaging

The transport outlined above in section 2.3.2 is known to overestimate the transport [64], but it was pointed out in Refs. [65–67] that the effect of finite Larmor radius as well as toroidal drift would reduce the diffusive transport. The basic idea is that the Larmor orbit and the drift orbit mean that the actual particle is circulating at a distance around the field line and effectively sees an average perturbation in the region, reducing the transport. The width of the drift orbits and Larmor orbits are related to the momentum of the particles, and continue to grow for relativistic energies, in contrast to the parallel streaming discussed in the section above. This difference in the relativistic generalisation suggests a maximal transport in the intermediate energy range.

As a result of the drift orbit width increasing linearly with the particle momentum, Ref. [62] observed a diffusion coefficient proportional to the inverse electron energy,

i.e. $(1+p^2)^{-1/2}$ for electron energies above 1 MeV in a perturbed magnetic field resulting from micro turbulence. The Larmor orbit becomes important if the gyro radius is comparable to the perpendicular magnetic correlation length, $\lambda_\perp$[4] as the orbit is no longer within a correlated region of the magnetic field perturbation. Ref. [68] showed that this effect becomes important, resulting in reduced transport, when

$$r_L > 0.36\lambda_\perp. \tag{2.32}$$

The transport gains an extra factor of inverse energy in the high energy region [62], resulting in a total scaling of the diffusion constant $(1+p^2)^{-1}$.

These diffusion coefficients now need to be introduced into the kinetic equation (2.19). We will work in the approximation that the toroidal geometry can be treated as a cylinder with toroidal symmetry. Furthermore we will only consider radial variations and not variation in the poloidal plane, assuming most plasma quantities remain almost independent of poloidal angle. The radial diffusion operator is added to the kinetic equation (2.19), resulting in

$$
\begin{aligned}
\frac{\partial \bar{f}}{\partial t} &= \frac{1}{\tau}\frac{\partial}{\partial p}\left[\left(-\xi E + p\nu_s + F_{\text{br}} + \frac{p\gamma}{\tau_{\text{syn}}}\left(1-\xi^2\right)\right)\bar{f}\right] \\
&+ \frac{1}{\tau}\frac{\partial}{\partial \xi}\left[\left(1-\xi^2\right)\left(-\frac{E}{p}\bar{f} + \frac{1}{2}\nu_D\frac{\partial \bar{f}}{\partial \xi}\right) - \frac{\xi\left(1-\xi^2\right)}{\tau_{\text{syn}}\gamma}\bar{f}\right] + \frac{1}{r}\frac{\partial}{\partial r}rD\frac{\partial \bar{f}}{\partial r}.
\end{aligned}
\tag{2.33}
$$

In the following chapter, we will propose a theory defining how the runaway avalanche growth rate without any effect of diffusion, γ_r, can be corrected to account for this effect. The corrected growth rate, γ, will be considered both when radiative effects are excluded, 3.1, and included, 3.2, for a general phase space-dependent diffusion coefficient $D(p)$. The corrections to the growth rate are discussed specifically for a diffusion coefficient inversely proportional to the particle momentum at high energies, in sections 3.4 and 3.5.1 as it allows a closed analytic form to be developed. In section 3.4 the effects of radiation on such a model are of particular interest. In section 3.5.2 the effects of models inspired by this section and 2.3.2 are considered to account for non-relativistic velocities and orbit averaging of the magnetic perturbation.

---

[4]The magnetic correlation length is defined as the length scale of the correlation function $\langle\delta B_\perp(x)\delta B_\perp(x+\delta)\rangle \sim e^{-\delta^2/2\lambda_\perp^2}$, where $\delta B_\perp$ is the radial perturbation of the magnetic field.

3

Reduction of avalanche growth rate by radial diffusion

The generation of runaway electrons tends to occur primarily in the central regions of the tokamak, in the hot region of the pre-disruption plasma, where the majority of the plasma current is driven. Diffusive transport will tend to move particles radially outwards towards the wall, spreading the runaways and inhibiting a localised build-up. When a runaway electron passes the last closed flux surface it will be on a trajectory towards the wall of the tokamak, where it will be lost from the plasma. Diffusion due to magnetic perturbations, arising or applied during a disruption, thus offers a potential runaway mitigation scheme. A finite diffusion could allow for a sufficiently small and spatially distributed flux of electrons to the wall without causing damage to the wall, whilst also inhibiting the avalanche, as the electrons will be lost before they have had time to multiply.

3.1 Growth rate correction without radiative effects

The effect of diffusion on the avalanche growth rate was first considered by Helander et al. [14]. We will present a summarised version of the calculation with some generalisations in this section, as it forms a crucial basis for the work presented in this thesis. To begin with, as was the case in Ref. [14], we will not consider terms corresponding to synchrotron and/or bremsstrahlung in the kinetic equation or spatial variations of either the electric field and/or the diffusion coefficient. These will be discussed in sections 3.2 and 5.1, respectively.

The appearance of the diffusion term in the kinetic equation adds another dimension to the problem, a radial one, compared to the "standard" growth rate calculation [23, 51]. Instead of solving the full problem, we will find an approximate solution with the aid of a separation of time scales. The avalanche generates secondary electrons with momentum rather close to p_c[1] and the time scale for an electron to be accelerated from this region up to relativistic momenta is $\tau_{\mathrm{acc}} \sim m_e c / e E_{\parallel} = \tau / E$ if the electric field is measured in units of E_c. The time scale of the avalanche growth is significantly longer, namely $\gamma_r^{-1} \sim \ln \Lambda \ \tau_{\mathrm{acc}}$. Thus if one has transport

---

[1]The avalanche source term is $\frac{1}{p^2} \frac{\partial}{\partial p} \frac{1}{\gamma - 1} \sim \frac{1}{p^5}$ for low momenta, and therefore does not extend far into the runaway region.

time scales significantly longer than the acceleration time scale, the diffusion will not be strong enough to alter the generation process, but may still hinder the avalanche.

To this end the momentum space is divided into a low energy region, $p < p_*$, where all the runaway generation occurs and the effects of diffusion are neglected, and a high energy region, $p > p_*$, where all the spatial diffusion takes place. The high energy region is fed with electrons from the low energy region and not directly from a source term (which is only present in the low energy region). Runaway electrons often have small pitch-angles, $\xi \approx 1$ and therefore the collision operator is expanded assuming $p_\perp \ll p_{||}$. The expansion of the terms of the kinetic equation involving pitch-angle derivatives are:

$$
\begin{aligned}
\frac{1}{2}\frac{\partial}{\partial \xi}(1-\xi^2)\frac{\partial f}{\partial \xi} &\approx \frac{p_{||}^2}{2p_\perp}\frac{\partial}{\partial p_\perp}p_\perp\frac{\partial f}{\partial p_\perp} + \mathcal{O}(f) \\
\frac{\partial}{\partial \xi}\frac{1-\xi^2}{p}f &\approx \left(\frac{\partial}{\partial p_{||}} - \frac{p_{||}}{p_\perp}\frac{\partial}{\partial p_\perp}\right)\frac{p_\perp^2}{p^2}f \sim \mathcal{O}(f),
\end{aligned}
\tag{3.1}
$$

where for the ordering we have assumed $\partial f/\partial p_{||} \sim f/p_{||}$ and $\partial f/\partial p_\perp \sim f/p_\perp$. Thus integrating the collision operator over momentum perpendicular to the magnetic field line annihilates the leading term of (3.1) and results in

$$
\int_0^\infty dp_\perp\, 2\pi p_\perp C(f) = \int_0^\infty dp_\perp\, 2\pi p_\perp \frac{1}{\tau p^2}\frac{\partial}{\partial p}(1+p^2)f \approx \frac{1}{\tau}\frac{\partial}{\partial p}F + \mathcal{O}(f/p^2), \tag{3.2}
$$

where only the leading order term in p is kept in the high energy region. The distribution function integrated over perpendicular momenta F has been introduced and is defined as

$$
F = \int d^2\boldsymbol{p}_\perp f = \int_0^\infty dp_\perp\, 2\pi p_\perp f. \tag{3.3}
$$

Integrating the kinetic equation (2.33) gives the rate of change of F in the high energy region as

$$
\tau\frac{\partial F}{\partial t} + (E-1)\frac{\partial F}{\partial p} = \tau\frac{1}{r}\frac{\partial}{\partial r}rD(p)\frac{\partial F}{\partial r}, \tag{3.4}
$$

where the diffusion coefficient for particles travelling purely along the magnetic field line is used to first order. This is the same time evolution equation as equation (12) in Ref. [14]. As the boundary condition is set by the avalanche mechanics at low momenta, where the effect of diffusion has been neglected, the flux of particles into the high energy region should be $\gamma_r n_{\mathrm{RE}}$. Here γ_r is the growth rate without the diffusion and n_{RE} is the spatial density of runaway electrons. As equation (3.4) is an advection equation without the presence of the diffusion, the boundary condition is[2]

$$
F(p_*) = \frac{\tau\gamma_r}{E-1}n_{\mathrm{RE}} = \frac{\tau\gamma_r}{E-1}\int_{p_*}^\infty dp\, F, \tag{3.5}
$$

which is not a typical boundary condition as the lower boundary in p is dependent on the solution in the whole region. Equation (3.4) may be solved if we use that the zeroth order Bessel modes $J_0(k_i r)$, with $k_i = b_i/a$ and b_i zeros to $J_0(x)$, are

---

[2]Consider an advection equation $\frac{\partial y}{\partial t} + \frac{\partial}{\partial x}(v(x)y) = 0$, the flow through a given point x is $v(x)y$.

eigenfunctions of the diffusion operator and form a basis set on the radial space with boundary condition $\frac{\partial F}{\partial r}|_{r=0} = 0$ and $F(a) = 0$ (corresponding to an absorbing wall at $r = a$) with measure $2\pi r dr$ [69]. Further if it is assumed that every mode is in quasi-steady state, i.e. is only scaled in time, the momentum part of the equation can be solved by the method of integrating factor and the solution can be written as

$$F(p, r, t) = \sum_{i=1}^{\infty} c_i J_0(k_i r) e^{\gamma_i t - \frac{\tau}{E-1} \int_{p_*}^{p} dp'(\gamma_i + k_i^2 D(p'))}, \tag{3.6}$$

where the coefficients $\{c_i\}_{i=1}^{\infty}$ are determined by the initial condition and the growth rate of the modes γ_i should be determined by the boundary condition.

In Ref. [14], only a single Bessel mode of the runaway electron density was considered, $i = 1$, which will be the least suppressed modes as higher mode numbers have a smaller characteristic length scale of variations and therefore will experience a larger diffusion. This corresponds to a conservative estimate of the effect of transport on the runaway dynamics. Here we choose to retain all of the modes, allowing us to propagate the profile in time. As a consequence of the orthogonality of the Bessel modes the boundary condition can be projected on each separated mode, decoupling the modes from one another. The equation for γ_i then follows from equation (3.5) as

$$1 = \frac{\gamma_r \tau}{E - 1} \int_{p_*}^{\infty} dp \, \exp\left(-\frac{\tau}{E - 1} \int_{p_*}^{p} dp'(\gamma_i + k^2 D(p'))\right). \tag{3.7}$$

The solution to this will be considered starting in section 3.3. Before we investigate the structure of this integral equation we will generalise this treatment of spatial diffusion in the kinetic equation to include radiation reaction forces, which were not considered in Ref. [14].

3.2 Growth rate correction with radiative effects and finite pitch-angle

The synchrotron radiation reaction force is strongly dependent on the momentum perpendicular to the magnetic field line as it is a consequence of the gyration around the field line. Therefore the $p_\perp$-dependence of the distribution function is no longer trivial to handle, as was done above in section 3.1, in a model where the effect of synchrotron radiation is included. Radiative effects are important close to the critical electric field where the acceleration from the electric field is close to being balanced by the radiation reaction forces, making the dynamics in the energy direction of momentum space comparatively slow. Therefore, as earlier done in Ref. [39, 70, 71] we will consider the pitch-angle dynamics to be a rapid process compared to the dynamics in energy. Thus we have an equilibrium in the pitch-angle distribution for a given p, requiring that the pitch-angle flux of particles vanishes. The condition for the pitch-angle flux to vanish follows from the kinetic equation (2.19) as

$$0 = \left(1 - \xi^2\right) \underbrace{\left(-\frac{E}{p}\bar{f} + \frac{1}{2}\nu_D \frac{\partial \bar{f}}{\partial \xi}\right)}_{=0} - \underbrace{\frac{\xi(1 - \xi^2)}{\tau_{\text{syn}}\gamma}\bar{f}}_{\text{neglected}}. \tag{3.8}$$

Since $\tau_{\mathrm{syn}} \gg 1$ we do not consider the effect of the synchrotron radiation on the pitch-angle distribution but rather just a balance between diffusive transport of the pitch-angle scattering and the collimating effect of the electric field. This approximation is strictly speaking only valid close to the point where the radiation balances the acceleration of the electric field, as the particle flux in the energy direction is otherwise important for the pitch distribution. As we later will observe, it is only close to the effective critical electric field, when this approximation is valid, that the radiative corrections will have a major influence, otherwise the electric field dominates the problem. Following from these conditions the distribution function may be written as

$$\bar{f} = F(r, p, t) \frac{A(p)}{2 \sinh(A(p))} e^{A(p)\xi}, \qquad (3.9)$$

where $A(p) = 2E/p\nu_D$ determines the extent of the distribution function in ξ. For large p, ν_D scales as $1/p^2$ and consequently the pitch-angle distribution becomes narrow in this limit as $A \propto p$, in agreement with the assumptions of section 3.1.

By performing the integration of the kinetic equation over pitch-angle a reduced kinetic equation is obtained

$$\frac{\partial F}{\partial t} + \frac{1}{\tau} \frac{\partial}{\partial p} (U(p)F) = \frac{1}{r} \frac{\partial}{\partial r} r \langle D \rangle_\xi \frac{\partial F}{\partial r}, \qquad (3.10)$$

where the pitch averaged acceleration force $U(p)$ is

$$U(p) = E \coth A - \left[\frac{p\nu_D}{2} + p\nu_s + F_{br} + \frac{p^2 \gamma \nu_D}{\tau_{\mathrm{sny}} E} \left(\coth A - \frac{1}{A} \right) \right], \qquad (3.11)$$

and the pitch-angle averaged diffusion coefficient is

$$\langle D \rangle_\xi(p) = \int_{-1}^{1} d\xi \, D(p, \xi) \frac{A e^{A\xi}}{2 \sinh A}. \qquad (3.12)$$

A qualitative difference between this model with the radiation reaction terms compared to the one without is the appearance of an upper limit of particle momenta, $p_{\max}$. This is the first appearance of a momentum above p_c where the forces due to radiation balance the acceleration from the electric field, corresponding to the momentum where the accelerating force U vanishes. Equation (3.10) may now be solved in the same manner as equation (3.4). The solution for the distribution function is given by

$$F(p, r, t) = \frac{1}{U(p)} \sum_{i=1}^{\infty} c_i J_0(k_i r) \exp \left(\gamma_i t - \int_{p_*}^{p} dp' \frac{\tau}{U(p')} \left(\gamma_i + k_i^2 \langle D \rangle_\xi(p') \right) \right), \qquad (3.13)$$

where once again the growth rate of the modes γ_i are determined by the boundary conditions. The lower boundary condition in momentum space is formed as above with the exception that the integration over p to form the total number of runaway electrons is limited by $p_{\max}$. Separated for every mode the boundary condition reads

$$1 = \int_{p_*}^{p_{\max}} dp \, \frac{\gamma_r \tau}{U(p)} \exp \left(- \int_{p_*}^{p} dp' \, \frac{\gamma_i \tau + \tau k_i^2 \langle D \rangle_\xi}{U(p')} \right). \qquad (3.14)$$

This condition for the growth rate has the same structure as (3.7) with the exception that the generalisation of the factor $E - 1$ to U is dependent on p and thus appears inside the integrals.

The solutions γ_i to the integral equation now depend on the properties of this force function $U(p)$. For large electric fields E, $U(p)$ has two roots which represent p_c and $p_{\max}$, between which the runaway region exists with positive acceleration. For lower electric field the runaway region shrinks and finally for electric field strengths E below some E_c^{eff} no solution to the equation $U(p) = 0$ exists and the runaway region disappears in such situations. Therefore, for electric field strengths below $E_c^{\text{eff, rad}}$ no runaway electrons will be generated, even when diffusion is not considered. Examples of the U-function for various E values in fully ionised plasmas can be seen in figure 3.1. It should be noted that the extent of the runaway region drastically varies close to $E_c^{\text{eff, rad}}$ and that, for large electric fields, $U(p)$ has a large region in momentum space where it is approximately $E - 1$, in agreement with the non-radiative theory.

The existence of $p_{\max}$ produces a singularity which lies on the edge of the integration region of equation (3.14). It needs to be treated with some care and this point will be discussed extensively in section 3.3 and 4.1. Likewise, a singularity appears at p_c - this point lies outside the integration region but its appearance can strongly affect the correction if p_* is not chosen significantly above p_c. The model presented for the radiation dynamics does not capture the behaviour close to p_c, as there the pitch-angle distribution becomes nearly isotropic rather than the shape described by equation (3.9), and the effect of the electric field is better described by a diffusive process in momentum space than an advective one [23]. We will therefore perform a large p-expansion of $U(p)$, which captures the effect of $p_{\max}$ but limits the impact of p_c. A large p-expansion keeping terms which grow with p results in

$$
\begin{aligned}
U(p) = E - \bar{\nu}_{s0} &+ \frac{\bar{\nu}_{D0}^2}{2\tau_{\text{sny}}E^2} - \left(\bar{\nu}_{s1} + \frac{\bar{\nu}_{D0}\bar{\nu}_{D1}}{\tau_{\text{syn}}E^2} \right) \ln p + \frac{\bar{\nu}_{D1}^2}{2\tau_{\text{syn}}} \ln^2 p \\
&- \left(\phi_{br0} + \frac{\bar{\nu}_{D0}}{\tau_{sny}E} \right) p - \left(\phi_{br1} + \frac{\bar{\nu}_{D1}}{\tau_{sny}E} \right) p \ln p
\end{aligned}
\tag{3.15}
$$

and ϕ_{br0} and ϕ_{br1} were defined by equation (2.18). This is compared to the full expression for $U(p)$ in figure 3.1a. If the logarithmic and quadratically logarithmic terms are neglected, $p_{\max}$ may be expressed in terms of the product log function $W(x)$ [3] as

$$
p_{\max} = \frac{a}{W\left(ae^b\right)},
\tag{3.16}
$$

with

---

[3]Also known as the Lambert function and it is the inverse to $f(W) = We^W$.
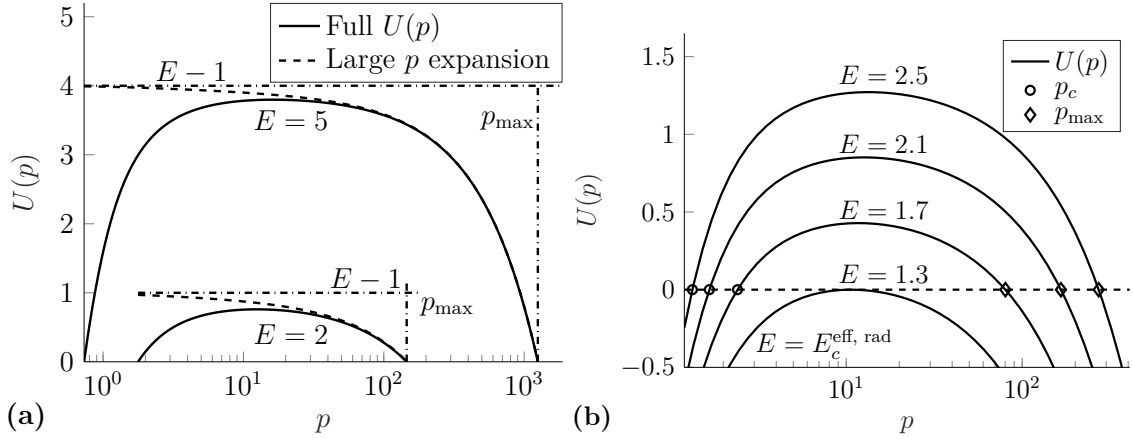
Figure 3.1: (a) Comparison between force function, $U(p)$ defined by (3.11), its large p-expansion, (3.15), and its counterpart in the non-radiative model, $E - 1$. (b) The position of p_c and p_{max} for different values of E. At $E = E_c^{\text{eff, rad}}$ the runaway region vanishes and $p_c = p_{max}$. Both illustrations correspond to plasma parameters $\ln \Lambda = 15$, $Z_{\text{eff}} = 1$, $n_e = 10^{20} \text{m}^{-3}$, $B = 1\text{T}$ and no screening effects.

$$a = \frac{E - \bar{\nu}_{s0} + \frac{\bar{\nu}_{D0}^2}{2\tau_{\text{syn}}E^2}}{\phi_{br1} + \frac{\bar{\nu}_{D1}}{\tau_{syn}E}}$$

$$b = \frac{\phi_{br0} + \frac{\bar{\nu}_{D0}}{\tau_{\text{syn}}E}}{\phi_{br1} + \frac{\bar{\nu}_{D1}}{\tau_{\text{syn}}E}}.$$

(3.17)

The approximation may be iteratively refined by evaluating the neglected terms at the approximate value of p_{max} and treating them as constants, shifting the a parameter.

3.3 Unification of the radiative and the non-radiative models

We will now consider the structure of the integral equations both in the non-radiative model (3.7) and in the radiative one (3.14), without specifying the phase space dependence of the diffusion coefficient. We will be able to map them to one another, allowing for an easier comparison. We define the dimensionless quantities which feature in the problem as,

$$x = \frac{\gamma\tau}{E - 1} \tag{3.18a}$$

$$x_r = \frac{\gamma_r\tau}{E - 1} \tag{3.18b}$$

$$\alpha(p) = \frac{\tau k^2 \langle D \rangle_\xi(p)}{E - 1}. \tag{3.18c}$$

The pitch-angle averaged diffusion coefficient was defined in equation (3.12), and reduces to $D(p)$ for a diffusion coefficient independent of pitch-angle ξ. Accordingly

x is the unknown representing the desired growth rate which should be solved for based on x_r and $\alpha(p)$. In this notation the implicit equations for the growth rate take the following forms,

$$1 = x_r \int_{p_*}^{\infty} dp \; e^{-\int_{p_*}^{p} dp' \; (x + \alpha(p'))} \qquad \text{(Non-radiative model)} \qquad (3.19\text{a})$$

$$1 = x_r \int_{p_*}^{p_{\max}} dp \; \frac{E-1}{U(p)} e^{-\int_{p_*}^{p} dp' \; \frac{E-1}{U(p')}(x + \alpha(p'))} \qquad \text{(Radiative model)}. \qquad (3.19\text{b})$$

In the non-radiative model, (3.19a), the electric field E and the diffusion coefficient D only appear through the ratio α. Therefore the same effect on the normalised growth rate is achieved by scaling down the diffusion coefficient or scaling up the electric field, and α sets the natural scale for the correction of x.

For the case of the model which includes the radiation reaction forces, (3.19b), the influence of the electric field is not purely through α, as U and $p_{\max}$ also depend on E. The factor $(E-1)/U(p)$ is close to order unity for a large portion of momentum space but becomes singular at $p_{\max}$, as was demonstrated in figure 3.1. Therefore the theory is not expected to differ from the case where radiative forces are neglected, unless $p_{\max}$ is at low enough momentum values, the electric field is close to its critical value, or when x is close to zero as the distribution function approximately decays in momentum space as $\sim \exp(-xp)/U(p)$.

A desirable property of the theory is to retrieve the uncorrected growth rate in the limit of no diffusion. This can readily be verified for the non-radiative model but will also be the case when radiation is treated. To show this the momentum coordinate q is introduced, defined by

$$q(p) = p_* + \int_{p_*}^{p} dp' \; \frac{E-1}{U(p')} \qquad (3.20)$$

in which the equation for x, (3.19b), takes the form

$$1 = x_r \int_{p_*}^{\infty} dq \; e^{-x(q-p_*) - \int_{p_*}^{q} dq' \; \alpha(p(q))}. \qquad (3.21)$$

The upper limit of the integral is infinite as q diverges as p approaches $p_{\max}$. The structure of this equation is exactly the same as for the theory without the influence of radiation, with the added complexity that the diffusion coefficient now is dependent on the inverse of (3.20), where q should be mapped to p. So technically, the change of variable maps one theory to the other, just with a different, but related, diffusion coefficient.

The added complexity of the inverse mapping can be ignored in the limit of no diffusion, as $D(p) = 0$. In this case the integrals in equations (3.19a) and (3.21) may be carried out analytically from which we conclude that the growth rates are equal, $x = x_r$. Thus we recover the uncorrected theory in the no diffusion limit.
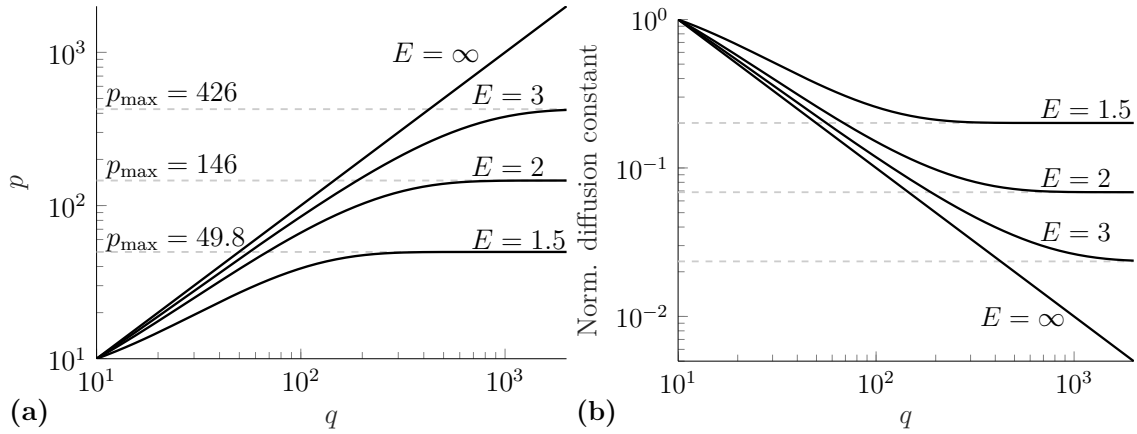
Figure 3.2: Examples of (a) the inverse mapping of (3.20) that transforms the radiative model to a non-radiative one and (b) the dependence of the diffusion coefficient on the new coordinate q, for a decreasing diffusion coefficient in momentum space of the form $(1 + p^2)^{-1/2}$. The illustrations of the transformation is based on the U presented in (3.11) evaluated with $Z_{\text{eff}} = 1$, $\ln \Lambda = 15$, $n_e = 10^{20}\text{m}^{-3}$ and $B = 1\text{T}$.

For non-zero diffusion coefficients, the general correction allowing for radiation is dependent upon the inverse mapping, $q \mapsto p$, for which we lack an explicit expression, but we can understand qualitatively. As q diverges when p goes to p_{max}, the inverse mapping saturates at p_{max} as q tends to infinity - consequently the value of the diffusion coefficient saturates to the value of $D(p_{\text{max}})$ for large q. This is exemplified in figure 3.2. The saturation of the diffusion coefficient determines for which x the generalised integral in equations (3.19a) and (3.21) converge, which sets a lower limit for the growth rate before the theory breaks down. Convergence is guaranteed if $x > -\alpha(p_{\text{max}})$ in the radiative model but depends on the large energy asymptote of α in the non-radiative theory - for most relevant diffusion coefficients the convergence criteria is $x \geq 0$.

The divergence of the theory is unphysical as it corresponds to an unbounded number of particles at high energies. It is an artefact due to there being no quasi steady-state solutions to the reduced kinetic equations, (3.4) and (3.10), from which the integral theory was derived. For a similar reason, one should be cautious before one uses the solution where x is particularly small, as the distribution function has the momentum space shape $\exp(-xp)/U(p)$, meaning that a large number of particles have large energy in such situations. It must be assessed if it is relevant to have such energetic particles based on the time the electrons has been accelerated.

To investigate the influence of different types of diffusion coefficients on the runaway problem a numerical algorithm solving the integral equations (3.21) has been implemented, but the detailed discussion of the methods used is deferred to chapter 4. In the remaining part of this chapter we will further investigate the general aspects of the growth rate correction, before considering the effects of specific diffusion models.

3.4 Effects of radiation on the growth rate correction

Radiation reaction forces will limit the maximum energy of a runaway electron and introduce a new momentum scale $p_{\max}$, where the acceleration from the electric field is balanced by the radiation. If $p_{\max}$ is large compared to p_c and p_* the effects of radiation will be limited, as most of the particles in a quasi steady-state distribution are located far below $p_{\max}$ and it is these particles which dominate the transport.

As demonstrated in figure 3.1b, $p_{\max}$ increases drastically with the electric field strength when it is above its critical value and the influence of this is seen on the solution of equation (3.21) in figure 3.3a. The correction to the growth rate in the radiative model is shown for two different field strengths, with a diffusion coefficient proportional to the inverse of the particle energy. A significant difference can be seen between the non-radiative model and the radiative one for $E = 1.5$, while the discrepancy is below a few percent for $E = 3$, demonstrating that radiation only has a significant effect for electric fields close to the effective critical one, as anticipated in section 3.2.

The derivations in 3.1 and 3.2 do not specify a particular value of p_*, and the dependence of the final growth rate based on the choice of p_* seen in figure 3.3a is undesirable. When this variation is comparable in size to the correction it limits the predictive power of the theory. Some variation occurs here due to the energy dependence of the diffusion for particles just above p_*. In section 3.5.2 we will investigate other diffusion models which could limit this effect by having a weaker diffusion at p_*. The radiative model has a strong dependence on p_* close to p_c which is a consequence of the limited electron acceleration close to p_c, but as was discussed in section 3.2, the theory underlying the derivation of $U(p)$ is not expected to be valid in the vicinity of p_c. Therefore to limit the effect of p_c on the theory, as demonstrated in figure 3.3a we propose to expand $U(p)$ for large p as shown in equation (3.15), hence some details of the effect of p_c are lost but the effect of $p_{\max}$ is retained, where the theory is valid.

The variation of p_c with the electric field strength is important to the dynamics of the electron runaway problem. This dynamics is desirable to model for the diffusion as well. Therefore we propose to set $p_* = p_c$ to include the changing size of the runaway region, but expand $U(p)$ in a large p expansion to limit the influence of the region close to p_c which is not modelled properly. The numerical solution of equation (3.21), using $p_* = p_c$, is shown in figure 3.3b with a fixed diffusion strength and demonstrating the dependence of the growth rate correction on the electric field strength. The effective growth rate is strongly affected by the diffusion and a new effective critical electric field appears for which the growth rate is corrected down to null, $\gamma = 0$.

The relative corrections in figure 3.3b shows the influence of diffusion but masks the fact that the physical growth rate scales with the electric field as $E - 1$. By
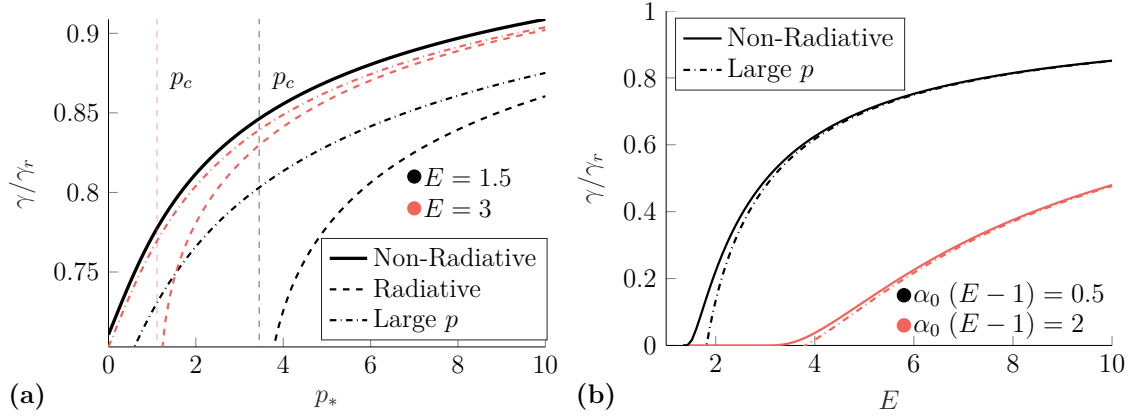
Figure 3.3: (a) Corrections of the growth rate due to a diffusion coefficient of the form (3.23) which is inversely proportional to the particle energy, for the three different radiation models; non-radiative, radiative and the radiative model expanded in large p. Two different electric field strengths are compared while $\alpha_0 = 0.3$ is kept fixed. In the case of $E = 1.5$, $p_{\text{max}} = 28$ and a significant difference is seen when radiative effects are included, while in the strong field case, $p_{\text{max}} = 261$ and radiation has a limited effect on the result. (b) Relative growth rate correction for the non-radiative and the large p-expansion of the radiative model, as a function of normalised electric field strength with a diffusion coefficient again of the form (3.23). The plasma parameters are $Z_{\text{eff}} = 1$, $\ln \Lambda = 10$, $n_e = 10^{20}\text{m}^{-3}$ and $B = 1\text{T}$.

instead considering the correction of the growth rate in absolute terms, we find that the model predicts a nearly constant offset to the growth rate, which is illustrated in figure 3.4. This can be understood by Taylor expanding equation (3.21) in small α, which results in

$$\gamma\tau = \gamma_r\tau - \underbrace{x_r \int_{p_*}^{\infty} dq \ e^{-x_r(p-p_*)}\alpha_{E=2}(p(q))}_{\text{Independent of } E \rightsquigarrow \text{offset}} \tag{3.22}$$

where $\alpha_{E=2}(p) = \alpha(p) \cdot (E-1)$ which is independent of E. To arrive at this form integration by parts has been used once and the correction $x - x_r$ is assumed to be of order α. The reduction of the growth rate will lessen the generation of runaway electrons and the fact that there is a new critical electric field for net runaway generation will have implications for the plateau phase in the final stages of the disruption mechanics. We will return to the critical electric field in section 4.3.

Finally here we note that plasmas with partially ionised atoms inherit extra dynamics from the atomic physics. For our purposes, the main effects are (a) electron collisions with partially ionised atoms have different characteristics from collisions with fully ionised atoms with the same net electric charge (screening), and (b) ionisation and recombination will alter the density of free electrons. For our model of diffusion due to magnetic perturbations (a) will alter the uncorrected growth rate, γ_r, as well as the collision frequencies ν_D and ν_s which appear in the U-function. The effect of (b) will be to alter E_c and τ and thus the normalisations of x_r and
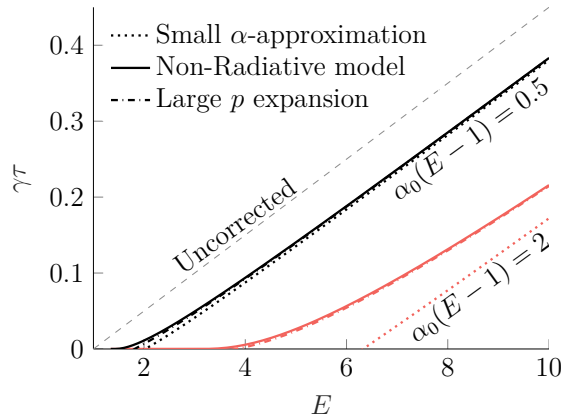
Figure 3.4: Comparison between the runaway growth rate in the different models in absolute units, as a function of normalised electric field. Taking $p_* = p_c$ has resulted in a small non-linear dependence of the small α-model for weak electric fields. Diffusion coefficient and plasma parameters are chosen as in figure 3.3b.

E. In principle, neither of these modifications alter the theory or the procedure for correcting the growth rate significantly. We will demonstrate the general effects of partially ionised ions in section 4.2 using the numerical solver for equation (3.21) presented in chapter 4.

3.5 Analytical treatment of diffusion models

In the literature there are two main treatments of the momentum space dependence of the diffusion coefficient, firstly by Rechester and Rosenbluth [13] treating the dependence of the speed of a particle and secondly, by Hauff and Jenko [62], considering orbit averaging effects, both of which we discussed in section 2.3. In this section we will treat the effect of the diffusion coefficient on the growth rate, using forms motivated by these studies.

3.5.1 p^{-1}-diffusion

For highly relativistic particles, with momenta predominantly along the magnetic field line, the diffusion coefficient is approximately inversely proportional to particle energy [62]. Therefore we will investigate a diffusion coefficient of the form

$$D(p) = \frac{D_0}{\sqrt{1 + p^2}} \tag{3.23}$$

and its implications on the effective growth rate. For this model some analytical progress can be made which can be used to test different limits of the full numerical solver developed in chapter 4. The fact that the integral over the high energy region of this diffusion coefficient diverges (non-radiative theory) is problematic for a prescription to correct the growth rate as outlined in equation (18) of Ref. [14], which circumvents actually solving the integral equation by assuming a rapid convergence

of the integral of the diffusion coefficient. Here we avoid this problem as we are solving the equation based on this specific diffusion coefficient.

Working in the non-radiative model, (3.19a), to avoid complications of the $U(p)$ function and using the dimensionless notation $\alpha(p) = \alpha_0/\sqrt{1+p^2}$ the inner integral of the integral equation (3.19a) can be performed analytically. No explicit expression for the resulting integral equation,

$$1 = x_r \int_{p_*}^{\infty} dp\, e^{-x(p-p_*)} \left(\frac{p_* + \sqrt{1+p_*^2}}{p + \sqrt{1+p^2}} \right)^{\alpha_0},\qquad(3.24)$$

has been found. To achieve an explicit expression for the corrected growth rate, x, we replace the integrand by its high and low energy asymptote as,

$$p + \sqrt{1+p^2} \longrightarrow \begin{cases} 1+p & \text{if } p < 1 \\ 2p & \text{if } p > 1. \end{cases}\qquad(3.25)$$

The approximation of the integrand is continuous but not smooth, which will be reflected in the final solution. Within this approximation the integral equation may be written in terms of the (upper) incomplete Γ-function $\Gamma(a,x)^4$ both for p_* larger and smaller then unity. Particularly if $p_* > 1$, equation (3.24) takes the form,

$$1 = x_r \int_{p_*}^{\infty} dp\, e^{-x(p-p_*)} \left(\frac{p_*}{p} \right)^{\alpha_0} = \frac{x_r}{x} e^{xp_*} (xp_*)^{\alpha_0} \Gamma(1-\alpha_0, xp_*),\qquad(3.26)$$

which we will expand in terms of small x, to obtain an explicit solution. The expansion in x is motivated as x_r is typically small, of the order $(2\ln\Lambda)^{-1}$, and at least for positive α, the spatial diffusion reduces the growth rate, $x < x_r$. Expanding equation (3.26) to leading order in x allows for an explicit solution,

$$x = p_*^{\frac{\alpha_0}{1-\alpha_0}} \left(\frac{\Gamma(2-\alpha_0) x_r}{x_r p_* + 1 - \alpha_0} \right)^{\frac{1}{1-\alpha_0}}.\qquad(3.27)$$

The equivalent steps can be conducted for $p_* < 1$ for which the growth rate is given by

$$x = \left(\frac{2^{\alpha_0} x_r \Gamma(2-\alpha_0)(1+p_*)^{\alpha_0}}{1 - \alpha_0 + x_r(1+p_*)^{\alpha_0} \left(2^{-\alpha_0} + (1+p_*)^{1-\alpha_0} - 2^{1-\alpha_0} \right)} \right)^{\frac{1}{1-\alpha_0}}.\qquad(3.28)$$

The explicit expressions, (3.28) and (3.27), clearly break down if $\alpha_0 = 1$, which is a consequence of the term in the expansion of equation (3.26) used to balance the equation becoming independent of x. The ordering of the equation is also violated if $\alpha_0 \geq 2$ limiting the use of the explicit expression in situations where the diffusion strongly influences the problem.

---

^{4}We use the following definition of the incomplete Γ-function; $\Gamma(a,x) = \int_x^{\infty} dt\, t^{a-1} e^{-t}$.
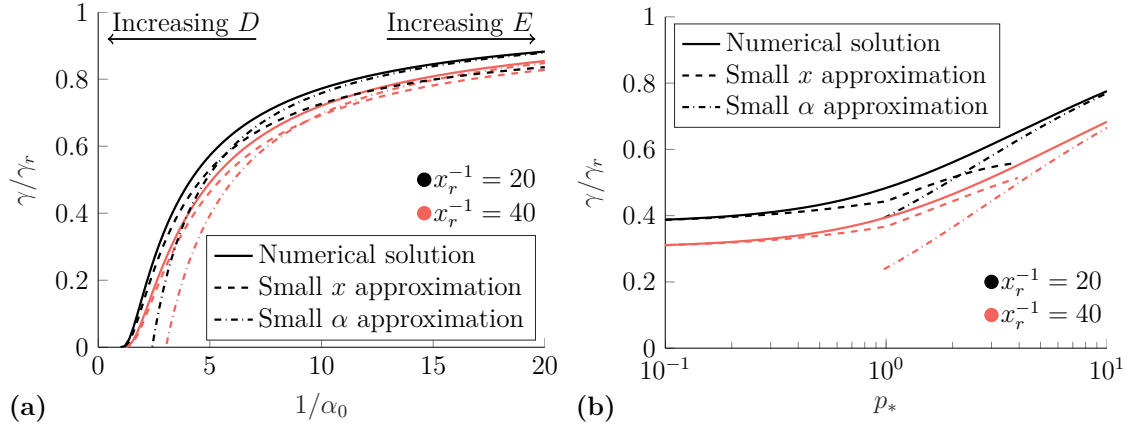
Figure 3.5: Comparison between the full numerical solution and the approximations based on a small x-expansion, equation (3.27) and (3.28), and a small α-expansion, equation (3.30). (a) As a function of α_0 with $p_* = 1$ and (b) as a function of p_* with $\alpha_0 = 0.2$.

The expansion in small x introduces a further constraint on α_0, originating from the assumption that higher order terms in x are small. This constraint reduces to

$$1 \gg (1 - \alpha_0)\Gamma(1 - \alpha_0)\left(\eta x\right)^{\alpha_0}, \tag{3.29}$$

where η for (3.27) is p_* and for (3.28), $\eta = \max\{2, p_*\}$, as a consequence of slightly different expansion parameters. Thus the expansion is not valid in the no diffusion limit. To handle this limit a direct expansion of the integral equation (3.19a) in small α can be conducted. Assuming the correction $x - x_r$ is of order α gives an expression for the correction in this limit as,

$$x = x_r \left(1 - \int_{p_*}^{\infty} dp \, e^{-x_r(p - p_*)}\alpha(p)\right), \tag{3.30}$$

which in the following we will call the small α approximation.

Both of the approximations above are compared with the full numerical solver in figure 3.5a, and are seen to agree with the full solution in their respective limits. In figure 3.5b the dependence of the theory on the free parameter p_* is demonstrated. The choice of p_* is seen to impact the prediction of the theory but also to be well described by the approximate expressions, especially for small p_*, understood by the condition (3.29). The small α approximation fits the full numerical solver better for larger p_* as the diffusion coefficient used is inversely proportional to particle energy and the maximum diffusion coefficient in the problem decreases as p_* is increased.

The development of these approximate expressions for the growth rate corrections is useful to understand the broad dependencies of the numerical solver and provide a quantitative comparison for the numerical solver. They would also be possible to implement in a larger fluid framework simulating the post disruption event essentially without added numerical cost, although the model limitations and validity

must be taken into account. The small α approximation can be appropriate during the current quench of disruptions with its large electric fields (but if the transport becomes large due to broken flux surfaces, this may not be the case) and the small x approximation is most fitting in the plateau phase where the runaway current is constant.

3.5.2 Non-monotonic diffusion models

If particles were to precisely follow a fully stochastic magnetic field, they would spread out spatially according to a diffusive process proportional to the particle velocity along the field line [13] as described in section 2.3.2. In the momentum coordinate system (p, ξ) the parallel velocity is,

$$v_{\parallel} = c\frac{\xi p}{\sqrt{1 + p^2}} \qquad (3.31)$$

and c is the speed of light. For the runaway electrons, which are typically highly relativistic and predominantly move in the parallel direction, this results in a constant diffusion coefficient. To combine the low energy dependence with the effects of drift orbit averaging [62] described in section 2.3.3, and earlier discussed in sections 3.5.1 and 3.4, a diffusion coefficient of the form

$$\alpha(p, \xi) = \alpha_0\frac{|\xi|\, p}{1 + p^2} \qquad (3.32)$$

is proposed which is a non unique interpolation between the two regimes. The normalisation of α_0 is chosen to agree with diffusion coefficient (3.23) for large energies in the forward direction. The pitch-angle averaging prescribed in section 3.2 results in a diffusion coefficient,

$$\langle\alpha\rangle_{\xi}(p) = \frac{\alpha_0 p}{1 + p^2}\frac{1}{2\sinh A}\left[\left(1 - A^{-1}\right)e^A - \left(1 + A^{-1}\right)e^{-A} + \frac{2}{A}\right]. \qquad (3.33)$$

where A^{-1} is the characteristic width parameter of the pitch-angle distribution according to equation (3.9). In such a model, where the diffusion is reduced compared to diffusion coefficients of the form (3.23), at momenta low compared to $m_e c$, the model is only weakly dependent on the choice of p_* below $m_e c$ but without significant alterations for $p_* > 1$. This is demonstrated in figure 3.6. Using this diffusion coefficient in the model proposed above in section 3.4, where $p_* = p_c$ and a large p-expansion of the $U(p)$-function is used, will limit the effect of the specific choice of p_* for large electric fields where p_c can be small compared to $m_e c$, but have limited effect otherwise.

The investigation of Hauff and Jenko [62] further shows a reduction of the diffusion coefficient for large energies, as the Larmor orbit is not within a correlated region of the magnetic field perturbation. The *Finite Larmor Radius* (FLR) effects become important at a critical pitch-angle ξ_{crit}, based on equation (2.32), which decreases with particle momentum as
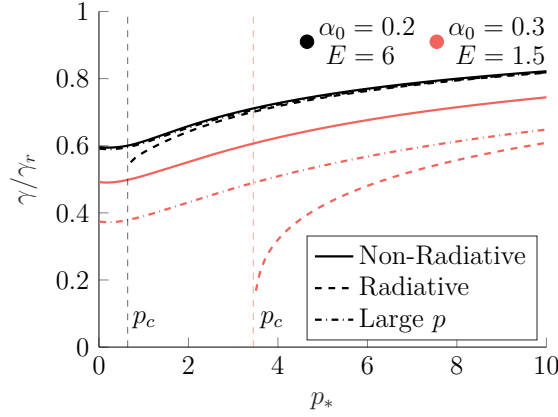
Figure 3.6: Relative correction of the growth rate as lower limit of the high energy region is varied, for diffusion coefficient of the form (3.33). The drastic changes in the low p_* region are suppressed compared to figure 3.3a if p_* is chosen below unity. This is a consequence of the particle velocity along the magnetic field line, which suppress the diffusion for momenta small compared to m_ec. Plasma parameters are onec again chosen as $Z_{\mathrm{eff}} = 1$, $\ln \Lambda = 15$, $n_e = 10^{20}\mathrm{m}^{-3}$, $B = 1\mathrm{T}$ and $x_r = (2\ln\Lambda)^{-1}$.

$$\xi_{\mathrm{crit}}^2(p) = 1 - \left(0.36\lambda_\perp \frac{eB}{mcp}\right)^2 \equiv 1 - \left(\frac{p_B}{p}\right)^2, \tag{3.34}$$

where we have defined $p_B = 0.36\lambda_\perp eB/mc$, the momentum scale at which particles can experience this increased suppression.

It is not reported over which range of pitch-angles this transition to a better confinement occurs and therefore we will assume a model where the transition is quick and discontinuous, i.e a diffusion model of the form,

$$D(p,\xi) = \begin{cases} \frac{D_0}{\sqrt{1+p^2}} & \xi > \xi_{\mathrm{crit}} \\ \frac{D_0}{1+p^2} & \xi < \xi_{\mathrm{crit}}. \end{cases} \tag{3.35}$$

without the additional dependence of the particle velocity introduced in (3.32) to begin with. The pitch-angle average of this model takes the form,

$$\langle D\rangle_\xi(p) = \frac{D_0}{2\gamma\sinh A}\left(\int_{-1}^{\xi_{\mathrm{crit}}} d\xi\, Ae^{A\xi} + \int_{-\xi_{\mathrm{crit}}}^{\xi_{\mathrm{crit}}} d\xi\, \frac{1}{\gamma}Ae^{A\xi} + \int_{\xi_{\mathrm{crit}}}^1 d\xi\, Ae^{A\xi}\right)$$
$$= \frac{D_0}{2\gamma\sinh A}\left(e^A + (\gamma^{-1}-1)e^{A\xi_{crit}} + (1-\gamma^{-1})e^{-\xi_{crit}A} - e^{-A}\right). \tag{3.36}$$

where $\gamma = \sqrt{1+p^2}$ is the Lorentz factor. The two different limits of (3.35) are obtained by $\xi_{\mathrm{crit}} = 0$ (corresponding to the limit $p_B \to 0$) and $\xi_{\mathrm{crit}} = 1$ ($p_B \to \infty$) respectively.

35

This correction to the diffusion coefficient is only influential if a significant fraction of particles have a larger pitch than the critical one, which is evidently the case if[5] $\xi_{\text{crit}} > 1 - A^{-1}$. The corresponding condition on p is,

$$\frac{E p_B^2}{1 + Z_{\text{eff}}} + \frac{1 + Z_{\text{eff}}}{4E} < p \tag{3.37}$$

where a large p-expansion of the deflection frequency of the form $\nu_D = (1 + Z_{\text{eff}})/p^2$ has been used. Consequently this region of increased suppression will influence the effective diffusion for large enough momentum given this model for the pitch-angle distribution. Figure 3.7a exemplifies the diffusion coefficient and equation (3.37) is seen to describe when the model differs from the diffusion coefficient in the forward direction.

This model has introduced a new undetermined parameter, p_B, related to the correlation length of the magnetic perturbation. Perturbations caused by turbulence are of the order of the ion gyro radius, ρ_i, and earlier investigations have used $\lambda_\perp = 2.5\rho_i$ [62]. Therefore in present day tokamaks, pre-disruption values of p_B could be in the range of ~ 5 while post-disruption values could be two orders of magnitude smaller. The actual magnetic field structure during the disruption is still largely unknown.

The numerical solutions for the growth rate corrections based on a diffusion constant of the form (3.36) are presented in figure 3.7b where a large range for the correction is observed based on the choice of the parameter p_B. In the large electric field limit all the models converge to the correction based on the diffusion in the forward direction, as the critical momentum where the increased suppression has a significant impact, quantified by (3.37), increases with the electric field strength[6].

For a combined model based on equation (3.32) and (3.35), which both accounts for the parallel particle speed and the finite pitch-angle of the electrons, we propose the following model,

$$\alpha(p, \xi) = \begin{cases} \alpha_0 \frac{|\xi| \, p}{1 + p^2} & \text{if } |\xi| > \xi_{\text{crit}} \\ \alpha_0 \frac{|\xi| \, p}{(1 + p^2)^{3/2}} & \text{if } |\xi| < \xi_{\text{crit}}. \end{cases} \tag{3.38}$$

The pitch-angle averaged diffusion coefficient based on this model,

$$\langle \alpha \rangle_\xi(p) = \frac{\alpha_0 p}{1 + p^2} \frac{1}{2 \sinh A} \left[\left(1 - A^{-1}\right) e^A - \left(1 - \gamma^{-1}\right) \left(\xi_{\text{crit}} - A^{-1}\right) e^{\xi_{\text{crit}} A} \right.$$
$$\left. + \left(1 - \gamma^{-1}\right) \left(\xi_{\text{crit}} + A^{-1}\right) e^{-\xi_{\text{crit}} A} - \left(1 + A^{-1}\right) e^{-A} + \frac{2\gamma^{-1}}{A} \right] \tag{3.39}$$

incorporates the characteristics of both (3.33) and (3.36) and where $\gamma = \sqrt{1 + p^2}$ is the Lorentz factor .

---

[5] Given the distribution function (3.9), this is the pitch angle where the distribution function has decreased by a factor of e^{-1} from its maximum.

[6] Which is the case when the electric field satisfies $E > 0.5(1 + Z_{\text{eff}})/p_B$.
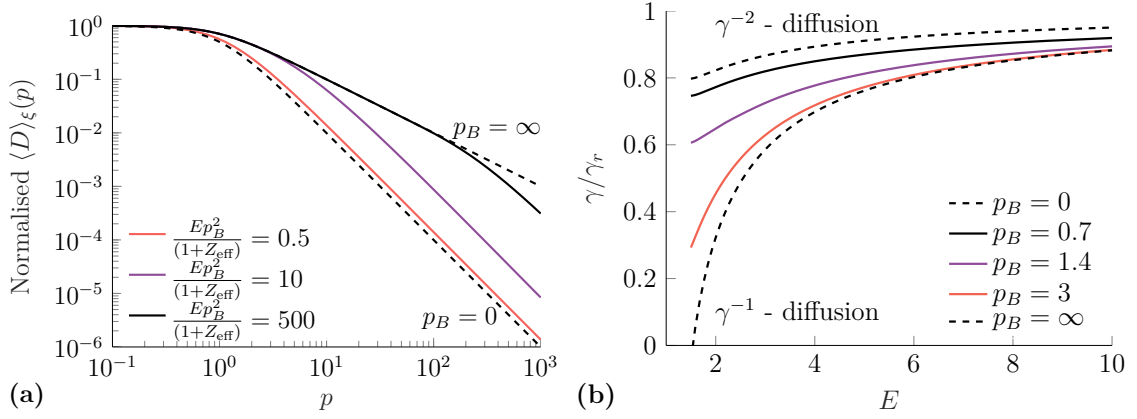
Figure 3.7: (a) Momentum dependence of the diffusion coefficient in the model which incorporates improves confinement from FLR effects, equation (3.36). The diffusion coefficient is seen to differ from the one in the forward direction for momentum as the condition (3.37) is satisfied. (b) The resulting relative correction of the growth for a set of values of p_B, as a function of electric field. The diffusion strength used is $\alpha_0 \cdot (E - 1) = 0.5$, a large p expansion model for $U(p)$ is used of the form (3.15), and $p_* = p_c$. Plasma parameters chosen as in figure 3.6.

To compute the correction of the growth rate for most shapes of the diffusion constant in momentum space a numerical algorithm is needed. Such an algorithm has been implemented solving (3.19a) and (3.21) for arbitrary diffusion coefficients and the method used will be discussed in the following chapter.

4

Numerical solution to the integral equations

The transport of runaway electrons does, in general, depend on the details of the magnetic field, and in non-stochastic fields it may differ from the tendencies outlined in section 2.3. In non-stochastic fields, there will still be transport as a result of drifts. This type of transport may be investigated by following the trajectories of test particles in the magnetic field under consideration. The resulting transport need not formally be a diffusive process, but the transport can often be represented by a combined advective and diffusive model [72]. To investigate the effect of the growth rate for the diffusion models presented in sections 2.3.2 and 2.3.3, as well as more general ones, there is a need for a general solver of the integral equations (3.19a) and (3.21). Below we will present such an algorithm.

4.1 Numerical scheme for growth-rate corrections

The numerical solver implemented for solving the integral equation (3.21)

$$1 = x_r \int_{p_*}^{\infty} dq \; e^{-x(q-p_*)-\int_{p_*}^{q} dq' \; \alpha(p(q))}. \tag{4.1}$$

can broadly be divided up into two parts, evaluation of the integrals for a given growth rate x and a root-finding algorithm. Before we further discuss the detail, we will list the major problems such a solver needs to overcome:

  i. The inner integral needs to be evaluated for a large set of endpoints. Moreover, the grid required for an accurate evaluation of the inner and outer integrals is often drastically different.
 ii. In the radiative model, both the inner and outer integral have a singular point at the upper integration limit, p_{max}, or the region close to p_{max} is mapped to an infinite region with the q-variable, defined in equation (3.20). This region needs to be treated separately for numerical accuracy.
iii. In the non-radiative model the upper boundary is infinity, $p_{max} = \infty$, and the integral needs to be truncated. The error of this truncation needs to be estimated and the truncation chosen accordingly.
 iv. The root-finding needs to be robust, as there is a point beyond which the integral does not converge, as well as minimising the number of function evaluations, as the integrals result in quite an expensive function to evaluate.

To address the first point in the list above, an ODE-solver has been used for calculating the inner integral as a function of its upper endpoint. A benefit of this approach is that there exist interpolation methods, accurate to the same order as the original ODE solver, which interpolate an ODE-solution on an arbitrary grid within the solution region. For the present problem, this allows for the use of different grids for the inner and outer integrals. An added benefit is that the inverse of the mapping (3.20) to the q-variable also can be formulated as an ODE and then the full system, consisting of the inverse mapping and the inner integral, can be treated as two coupled ODEs.

Concretely, we define a function $\mathcal{G}$ as,

$$\mathcal{G}(q) = e^{-\int_{p_*}^{q} dq'\ \alpha(p) - \alpha(p_{\max})} \tag{4.2}$$

which is dependent on the inverse map $p = p(q')$. Differentiating the definition of q, equation (3.20), and $\mathcal{G}$ gives the following coupled ODEs,

$$\frac{\partial}{\partial q} \begin{bmatrix} p \\ \mathcal{G} \end{bmatrix} = \begin{bmatrix} U(p)/\left(E-1\right) \\ -\left(\alpha(p) - \alpha(p_{\max})\right)\mathcal{G} \end{bmatrix} \quad \text{with} \quad \begin{bmatrix} p(p_*) \\ \mathcal{G}(p_*) \end{bmatrix} = \begin{bmatrix} p_* \\ 1 \end{bmatrix} \tag{4.3}$$

which any ODE-solver able to handle vector valued functions can solve. The $\mathcal{G}$ function is independent of the corrected growth rate x, the unknown in the problem, and therefore only needs to be computed once. Based on the definition of $\mathcal{G}$, we introduce a second function $f(x)$, whose root is the solution to the integral equation (3.21). The function f and its derivative are defined as

$$f(x) = x_r \int_{p_*}^{\infty} dq\ e^{-\Gamma(q-p_*)}\mathcal{G}(q) - 1 = \frac{x_r}{\Gamma} \int_0^1 d\lambda\ \mathcal{G}(q_\Gamma(\lambda)) - 1 \tag{4.4a}$$

$$f'(x) = -x_r \int_{p_*}^{\infty} dq\ (q-p_*)\, e^{-\Gamma(q-p_*)}\mathcal{G}(q) = \frac{x_r}{\Gamma^2} \int_0^1 d\lambda\ \ln\lambda\ \mathcal{G}(q_\Gamma(\lambda)) \tag{4.4b}$$

where $\Gamma = x + \alpha(p_{\max})$ and $q_\Gamma(\lambda) = p_* - \Gamma^{-1}\ln\lambda$. In the second equality a change of variables $\lambda = \exp\left(-\Gamma\left(q - p_*\right)\right)$ has been performed, which trivialises the exponential part of the integral and maps the integration region to a finite one. The variable Γ is dependent on x and therefore effectively different grids would have been used if a linear grid would have been used to evaluate the integral.

Since the $\mathcal{G}$-function generally is expensive to evaluate, it is desirable to only evaluate it once. Therefore $\mathcal{G}$ is evaluated on a q-grid which is mapped to different λ-grids dependent on x, i.e the same function values are kept but their position on the λ-axis is changed dependent on x, a process which is illustrated in figure 4.1. The grid in q is chosen based on the original ODE-solution of $\mathcal{G}$ because it accounts for the variations of $\mathcal{G}$. This grid in q is then filled out with an interpolation method for a more accurate evaluation of $f(x)$.

To address the second point in the list, an analytic approximation was made to treat the high energy tail of the integral equation in the radiative model. It is problematic to evaluate $\mathcal{G}$ for arbitrarily large q and therefore the integral is divided at a
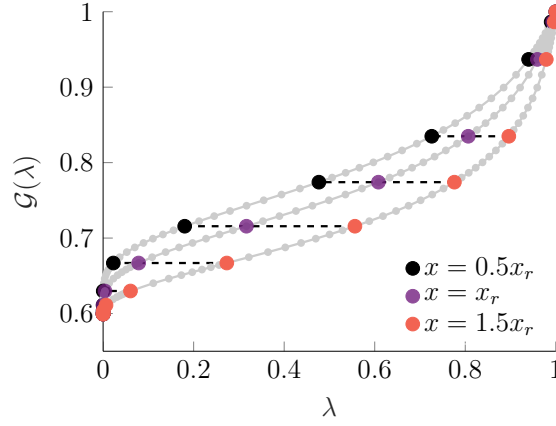
Figure 4.1: Illustration of how the $\mathcal{G}$-function, defined in equation (4.2), is calculated on a fixed grid in q which is transformed to $\lambda = \exp\left(-\left(x + \alpha(p_{\max})\right)(q - p_*)\right)$ for different values of x. The function values are kept fixed as their position on the λ-axis is changing for different x. The larger markers are the original adaptive grid from the ODE solver and the minor markers are the interpolated points.

momentum q_{ref}, into a low energy region $q < q_{\mathrm{ref}}$ which is integrated numerically, and a high energy region $q > q_{\mathrm{ref}}$ for which an analytic expression is found, based on saturation of the diffusion coefficient as demonstrated in figure 3.2b and a Taylor expansion of $U(p)$ and $D(p)$ close to $p_{\max}$. The introduction of q_{ref} divides the integral formulated in the p variable at some momentum p_{ref} which should be chosen close enough to $p_{\max}$ such that a first order Taylor expansion is valid in the region between p_{ref} and $p_{\max}$.

By definition of $p_{\max}$, $U(p_{\max}) = 0$ and the first order Taylor expansions of $U(p)$ and $\alpha(p)$ are

$$U(p) \approx U'(p_{\max})(p - p_{\max}) \equiv U_1(p_{\max} - p) \tag{4.5a}$$

$$\alpha(p) \approx \alpha(p_{\max}) + \alpha'(p_{\max})(p - p_{\max}) \equiv \alpha_{\max} + \alpha_1(p_{\max} - p) \tag{4.5b}$$

where U_1, $\alpha_{\max}$ and α_1 are positive constants in the typical case. Utilising the expansions and the integral definition of $\mathcal{G}$, the high energy region of (4.1) is evaluated by moving back to the p variable as

$$
\int_{q_{\mathrm{ref}}}^{\infty} dq\, e^{-(x+\alpha_{\max})(q-p_*)}\mathcal{G}(q)
$$

$$
\approx \frac{\mathcal{G}(q_{\mathrm{ref}})}{e^{(x+\alpha_{\max})(q_{\mathrm{ref}}-p_*)}}\frac{E-1}{U_1(p_{\max}-p_{\mathrm{ref}})}\int_{p_{\mathrm{ref}}}^{p_{\max}} dp\,\left(\frac{p_{\max}-p}{p_{\max}-p_{\mathrm{ref}}}\right)^{a-1} e^{-b\frac{p-p_{\mathrm{ref}}}{p_{\max}-p_{\mathrm{ref}}}}
\tag{4.6}
$$

where the constants $a = \frac{E-1}{U_1}(x + \alpha_{\max})$ and $b = \frac{\alpha_1(E-1)}{U_1}(p_{\max} - p_{\mathrm{ref}})$ have been defined. By the introduction of the dimensionless variable $s = (p_{\max} - p)/(p_{\max} - p_{\mathrm{ref}})$ the only dependence left on p_{ref} is through the parameter b. Finally integration by
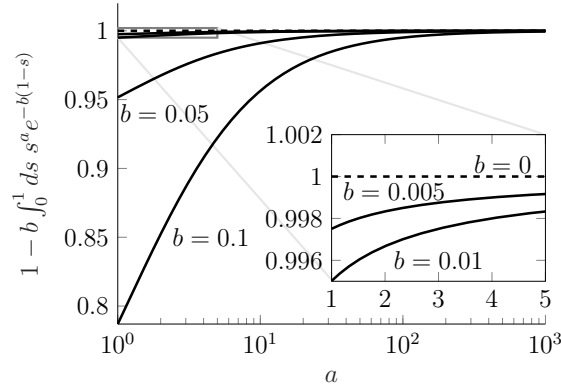
41

Figure 4.2: The singularity correction relative to the correction in the $b \to 0$ limit, plotted as a function of a for a set of finite b. As b can be chosen almost arbitrarily small it is valid to neglect the integral part of equation (4.7).

parts results in a regular integrand and a formulation suitable for numerical evaluation,

$$
\int\limits_{q_{\text{ref}}}^{\infty} dq \; e^{-(x+\alpha_{\text{max}})(q-p_*)} \mathcal{G}(q)
$$
$$
\approx \frac{\mathcal{G}(q_{\text{ref}})}{e^{(x+\alpha(p_{\text{max}}))(q_{\text{ref}}-p_*)}} \frac{E-1}{U_1} \left[\frac{1}{a} - \frac{b}{a} \int_0^1 ds \; s^a e^{-b(1-s)} \right].
\tag{4.7}
$$

The b dependent part of the integral is related to the variation of the diffusion coefficient close to p_{max} which should not impact this region significantly. An order of magnitude estimation given a model where $D \sim \alpha_0/p$ confirms this as

$$
\begin{cases} U_1 \simeq \frac{E-1}{p_{\text{max}}} \\ \alpha_{\text{max}} \simeq \frac{\alpha_0}{p_{\text{max}}} \\ \alpha_1 \simeq \frac{\alpha_0}{p_{\text{max}}^2} \end{cases}
\implies
\begin{cases} a \simeq x p_{\text{max}} + \alpha_0 \\ b \simeq \alpha_0 \left(1 - \frac{p_{\text{ref}}}{p_{\text{max}}} \right) \end{cases}
\tag{4.8}
$$

and the b dependent part may be neglected if p_{ref} is chosen close to p_{max}. This point is further motivated in figure 4.2 where the dependence of (4.7) on b is explicitly shown. In the $b \to 0$ limit an algebraic expression for the tail of the integral in the integral equation (4.7) is obtained, which only depends on p_{ref} through a pre-factor, which will suppress this contribution as p_{max} increases. Therefore this contribution is primarily important for low electric fields where the effects of radiation are significant.

Just as we cannot evaluate the $\mathcal{G}$-function easily for arbitrarily large q, we need to introduce a cut-off for p in the non-radiative model. The calculation above is not valid in this case as it is dependent on the saturation of the diffusion constant as q tends to infinity. Instead, we will truncate the integral and estimate the error.

For diffusion coefficients that decay for large momenta, motivated by the discussion in section 2.3.3, an upper limit of the truncation error is arrived at by considering

the diffusion coefficient as constant in the truncated region. The imposed error in the solution for x from the truncation is,

$$I_T = \frac{\left| x_r \int_{p_{\max}}^{\infty} dp \, \mathcal{G}(p) e^{-(x+\alpha(p_{\max}))(p-p_*)} \right|}{|f'(x)|} \leq \frac{x_r \mathcal{G}(p_{\max})}{x + \alpha(p_{\max})} \frac{e^{-(x+\alpha(p_{\max}))(p_{\max}-p_*)}}{|f'(x)|} \quad (4.9)$$

where the correction to the derivative is assumed to be a small effect, as it would give the same error term multiplied by the percentile error in the derivative. If the error in x is not below the desired tolerance, ϵ_{tol}, a qualified guess for the necessary $p_{\max}$ is

$$p_{\max} \geq p_* - x^{-1} \ln \left(\epsilon_{tol}/I_T \right) \quad (4.10)$$

based on which the numerical evaluation of the integral and solver can be run again to arrive at a solution within the tolerance.

The last point in the list relates to a root-finding algorithm for the equation $f(x) = 0$. A Newton-Raphson method was implemented, as it gives quadratic convergence [73] and the derivative of $f(x)$ can be evaluated similarly to the function itself. As the solver is intended to be used in a larger framework, it needs to be unconditionally stable and converge to the solution in any case, especially as the function is rather ill-behaved close to the convergence limit, $x = -\alpha(p_{\max})$.

Unconditional stability is obtained by combining the Newton-Raphson method with the bisection method. The solution is first bracketed by considering α to be a constant function at its minimum $\alpha_{\min}$ and its maximum $\alpha_{\max}$ in the interval $[p_*, p_{\max}]$, in which case the integral equation (3.21) can be solved analytically, yielding the lower and upper bounds for the solution, $x_{\min} = x_r - \alpha_{\max}$ and $x_{\max} = x_r - \alpha_{\min}$ respectively. Then a Newton step is tested. If the next approximate solution from the Newton algorithm falls within the bracketed interval of the solution, it is kept and the interval updated based on the sign of f. If the approximate solution falls outside the interval the solver falls back on the bisection algorithm for one step. This was then iterated until convergence.

This root-finding algorithm inherits the unconditional stability from the bisection algorithm and the quadratic convergence close to the solution from the Newton-Raphson method. The draw-back is the non-optimal bisection steps, as extra function evaluations are needed to test the validity of a Newton step. Therefore, in practice, the solver first performs a couple of pure bisection steps to have a better initial guess for the solution. The use of this algorithm is demonstrated in the following section, where diffusion in the presence of partially ionised ions is investigated.

4.2 Radial transport in partially ionised plasmas

Partially ionised ions will affect the collisional dynamics in the plasma, as the fact that some electrons are in a bound state introduces an energy dependent change to the slowing down rate ν_s and the pitch angle scattering rate ν_D. The rate of diffusion considered here, which originates mainly from collisionless motion in perturbed magnetic fields, will not be severely altered, although the uncorrected growth rate γ_r and the acceleration function $U(p)$ are modified, as outlined at the end of section 3.4.

The numerical solver described in the previous section was used to produce figure 4.3, which shows a study of the correction due to diffusion on the growth rate in a partially ionised plasma, where $p_* = p_c$ and a large p-expansion of $U(p)$ has been used. A plasma mixture of deuterium and argon has been used for demonstration. The ionisation states were assumed to be in thermal equilibrium based on recombination and ionisation rates provided by Ref. [74]. The uncorrected growth rate was calculated from equation (2.26) which gives x_r a non trivial dependence on temperature and electric field as is shown in figure 4.3a. Ionisation and recombination will alter the density of free electrons in the system, altering E_c with temperature.

The corrected growth rate inherits the temperature dependence of the uncorrected one. Otherwise the trends for a varying electric field follow what is expected from figure 3.3b, where a constant x_r was investigated. This could be expected as x_r is only rapidly varying close to the effective critical electric field without the influence of transport. In a model including radiation reaction forces the effective critical electric field above which runaways are generated is larger than E_c, which will be labelled $E_c^{\text{eff, rad}}$. The critical electric field in the presence of radial diffusion (and radiation reaction forces) is where the growth is nullified by the transport $\gamma = 0$, which we will call E_c^{eff}. The critical electric field in the presence of diffusion is generally larger than $E_c^{\text{eff, rad}}$ as there can be a flux of runaway electrons through p_* which are then lost through spatial diffusion.

The scan in figure 4.3 shows how diffusion primarily has an effect at low electric fields and especially the appearance of a new effective critical electric field is significant. The two following sections will look into this question of a larger critical electric field, both how to find it numerically and predictions using the diffusion models presented in section 3.5.

4.3 Numerical calculation of critical electric field

The electric field at which the transport losses are balanced by the generation of runaway electrons from the avalanche process is the effective critical electric field E_c^{eff}. This is of specific interest for the runaway plateau in the final stages of a disruption [39, 75]. The time evolution of the electric field is governed by the inductive equation (2.24), where the electric field is set by the rate of change of the plasma current. As E_c^{eff} denotes the threshold electric field where the generation is matched
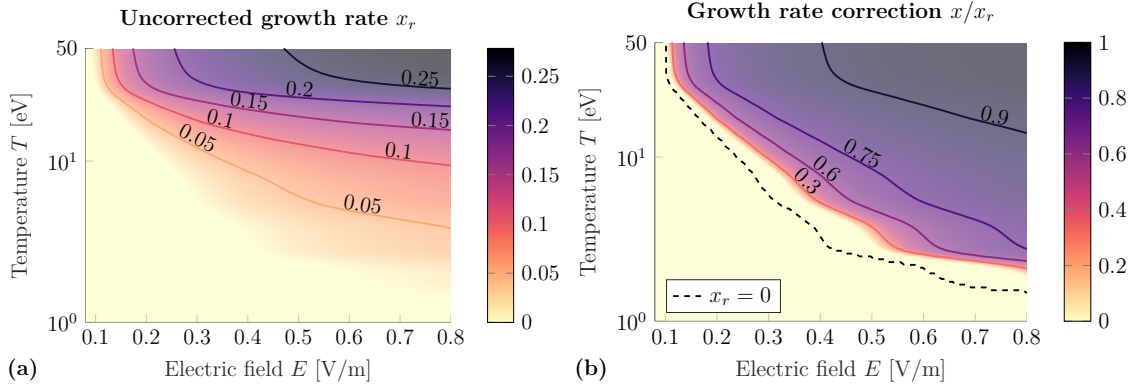
Figure 4.3: (a) Uncorrected growth rate in a plasma consisting of deuterium and argon with respective densities $n_\mathrm{D} = 10^{20}\mathrm{m}^{-3}$ and $n_\mathrm{Ar} = 0.3 \cdot 10^{20}\mathrm{m}^{-3}$ calculated from equation (2.26). The densities of the different ionisation degrees based on thermal equilibrium distribution. (b) Relative correction of the growth rate based on a diffusion model of the form (3.23) and $\alpha_0 \cdot (E - 1) = 1$, emulating a situation with a fixed diffusion strength. The dashed line shows the critical electric field without diffusion, whilst the critical electric field is seen to be higher when diffusion is accounted for. For both (a) and (b) a magnetic field strength of 5.3T is used.

by the losses, the electric field has a tendency to stabilise around this value. The balancing around E_c^eff predicts a strong correlation between the current decay time in the plateau phase and the plasma density, which is observed experimentally [76].

To find E_c^eff the numerical solver presented in section 4.1 could be wrapped in another root-finding algorithm solving $x(E) = 0$. A more efficient method is obtained by explicitly setting $x = 0$ in equation (3.21) and solving for the electric field. Since most parameters in the integral implicitly depend on E, it is challenging to evaluate derivatives with respect to E. We therefore implemented a *false position* method [77] based purely on function evaluations, which provides unconditional stability with an improved convergence compared to a bisection method. The false position method is a variant of the bisection method, which instead of bisecting the interval in every iteration, divides the interval by finding the root of the secant to the function between the interval endpoints. Close to the root the secant is a good approximation for the derivative of the function, improving convergence.

To solve the integral equation (3.19b) under the condition $x = 0$, the root to the function $f(E)$,

$$f(E) = x_r \int_{p_*(E)}^{p_{\max}(E)} dp \, \frac{E - 1}{U(p; E)} e^{- \int_{p_*(E)}^{p} dp \, \frac{E-1}{U(p;E)} \alpha(p;E)} - 1 \qquad (4.11)$$

needs to be computed. The function evaluation can be performed in the same manner as detailed in section 4.1, but the draw-back here is that the $\mathcal{G}$-function needs to be computed for every function evaluation, resulting in a significantly heavier function to evaluate. Therefore to improve convergence the *Anderson-Björck* im-
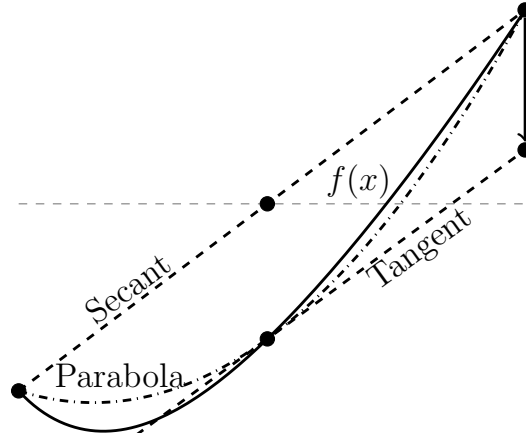
45

Figure 4.4: Schematic representation of the Anderson- Björck algorithm used if two following approximate solutions have the same sign of the function. Looking for the root of the function (solid line), the secant (dashed line) is drawn between the interval endpoints to approximate the solution. One of the endpoints is corrected such that the secant in the following iteration is the tangent (dashed line) at the current approximate solution to the parabola through the endpoints and the function evaluated at the current approximate solution (dot-dashed line).

provement [78] to the false position method was implemented [77]. If the function $f(E)$ has a constant sign on its second derivative, in the interval under consideration, the false position method will always give an estimate of the root on the same side of the real root, resulting in linear convergence. To prevent this the Anderson-Björck algorithm scales the function value at the endpoints by a method schematically described in figure 4.4 [73].

The false position method requires an upper and lower bound for the solution. As $f(E)$ is an increasing function for large electric fields, typically as shown in figure 4.5a, the upper limit for the solver was retrieved by successively testing larger electric fields until $f(E)$ is positive with a positive derivative. If a lower bound for E_c^{eff} is not found during this, $f(E) < 0$, a *Golden-section search* algorithm [79] searches for the minimum of $f(E)$ until a lower bound is found. This process is illustrated in figure 4.5a where the steps of the solver are shown step-by-step. Figure 4.5b shows the convergence of the algorithm in a test case and demonstrates the quicker convergence of the Anderson-Björck algorithm compared to a bisection method.

4.4 Effective critical electric field

The corrected critical electric field E_c^{eff} is the electric field which solves equation (3.21) under the condition $x = 0$. To resolve the ambiguity of p_* we will in this section use the model presented in section 3.4, where $p_* = p_c$ as well as using a large-p expansion for $U(p)$ according to equation (3.15). For large electric fields the effect of $p_{\max}$ is limited as it becomes much larger than the average particle momentum,
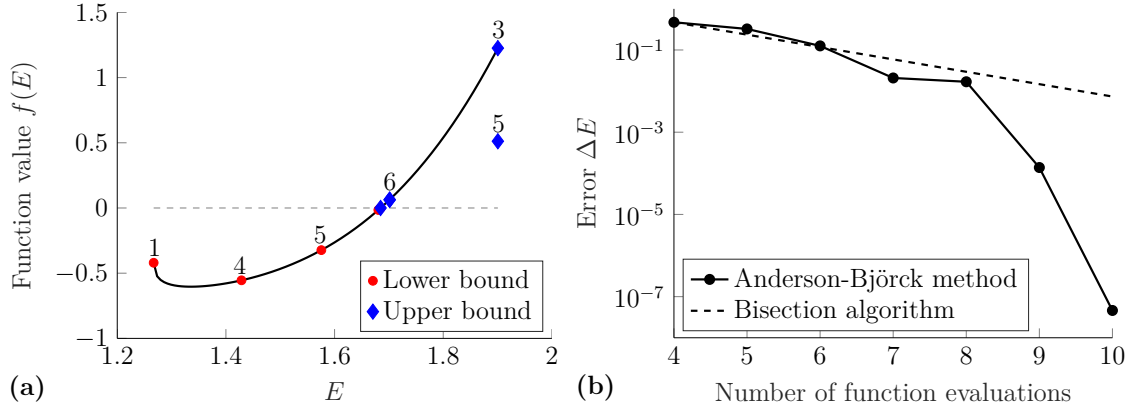
Figure 4.5: (a) A step-by-step look at the critical electrical field solver. Markers show where the function is evaluated and at which function evaluation it was computed. At function evaluation 5, the Anderson-Björck correction was made. (b) Convergence of the critical electric field solution with function evaluation, after a bracketed interval has been established. The solver is compared to the convergence of the bisection algorithm.

and p_c is only slowly changing with the electric field strength. Therefore the primary dependence on the electric field strength is through α which is proportional to some diffusion strength

$$\alpha(p) \cdot (E - 1) = \tau k^2 \langle D \rangle_\xi (p) \tag{4.12}$$

and inversely proportional to $(E - 1)$. So for a constant x_r there is an α which solves the equation $x = 0$, which means that there will be a linear relation between E_c^{eff} and the diffusion strength. This will be apparent later on when we look at the numerical solutions for E_c^{eff}. Physically this means that the correction to E_c^{eff} scales as $(\delta B / B)^2$ for the diffusion models presented in section 2.3. Furthermore, the critical electric field should scale quadratically with $k \sim 1/L$, with L the characteristic length scale of radial variations in the runaway electron profile. In units of E_c the correction is seen to have a linear dependence on τ as well, which would impose a density scaling - but this is not expected in physical units as the product τE_c is only dependent on natural constants.

In this model the runaway region disappears at an effective critical electric field, $E_c^{\text{eff, rad}}$, due to radiation reaction forces. This is the effective critical electric field in the growth rate formula (2.26) and for our model of correcting the growth rate to match this in the no diffusion limit, x_r needs to be zero at $E_c^{\text{eff, rad}}$. Therefore we use the growth rate formula (2.26) for complete screening, in the definition of x_r (3.18b) which gives,

$$x_r = \frac{(\ln \Lambda)^{-1}}{\sqrt{5 + Z_{\text{eff}}}} \frac{E - E_c^{\text{eff, rad}}}{E - 1} \tag{4.13}$$

where E and $E_c^{\text{eff, rad}}$ are both measured in units of E_c. The critical electric field for a p^{-1}-diffusion model is shown in figure 4.6a and the linear relation between diffu-
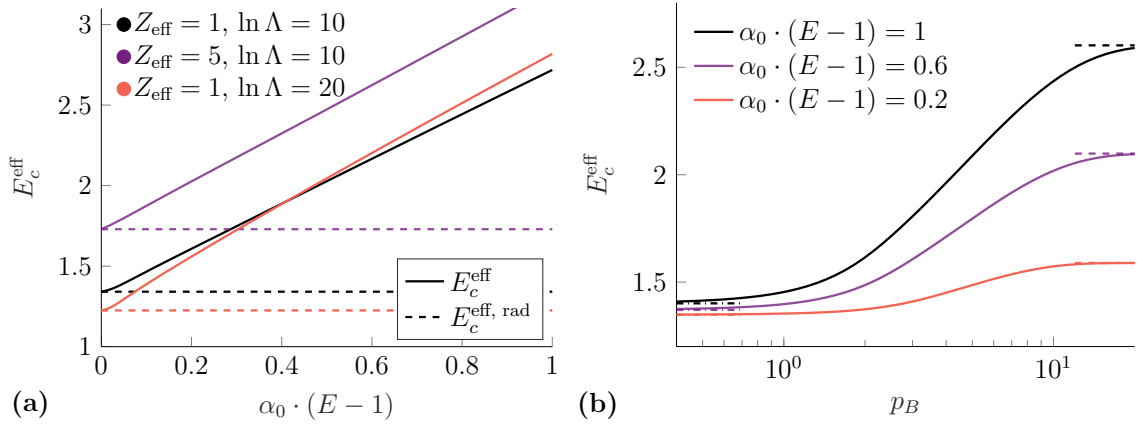
Figure 4.6: (a) Effective critical electric field for a diffusion model of the form (3.23) where $p_* = p_c$ and a large p-expansion of $U(p)$ has been used. A linear relation with diffusion strength is seen for large electric field, with a non-linear region close to $E_c^{\text{eff, rad}}$ such that the model matches the purely radiative theory in the no diffusion limit. (b) Critical electric field for a diffusion model of the form (3.39) as a function of p_B, related to the magnetic perturbation correlation length $\lambda_\perp$ as defined in equation (3.34). The limits $p_B = \infty$ (dashed line) and $p_B = 0$ (dot-dashed line) show the critical electric field for a model where $D \sim p^{-1}$ and $D \sim p^{-2}$ for large p, respectively. The transition between the two limits occurs for $p_B \in [1, 10]$. Plasma parameters are $\ln \Lambda = 10$ and $Z_{\text{eff}} = 1$.

sion strength and E_c^{eff} is obvious for large field strengths, but for small electric fields a non-linearity allows E_c^{eff} to match the purely radiative theory in the no-diffusion limit.

The critical electric field for a diffusion model which incorporates both the speed of the particles and orbit averaging effects, with a diffusion coefficient of the form (3.39), is investigated in figure 4.6b. The model is seen to go between its limits over an order of magnitude of the parameter $p_B = p_B(\lambda_\perp)$, which incorporates the effect of the correlation length of the magnetic perturbation. The limit $p_B \to 0$, where the diffusion coefficient for large p scales as $D \sim p^{-2}$, has only a slightly larger critical electric field than the purely radiative theory, compared to the $p_B \to \infty$ limit, where the energetic particles are less well confined with a diffusion coefficient scaling as $D \sim p^{-1}$.

The same procedure as in section 4.2 can also be performed for the critical field calculation, i.e the uncorrected growth rate can be calculated based on (2.26) for a plasma in thermal equilibrium. The same situation as was investigated in figure 4.3, with a plasma mixture of deuterium and argon is considered in figure 4.7, but focusing on the critical electric field. The effective critical electric field in the presence of diffusion inherits the features of the purely radiative theory but is offset at a larger field strength, dependent on temperature.
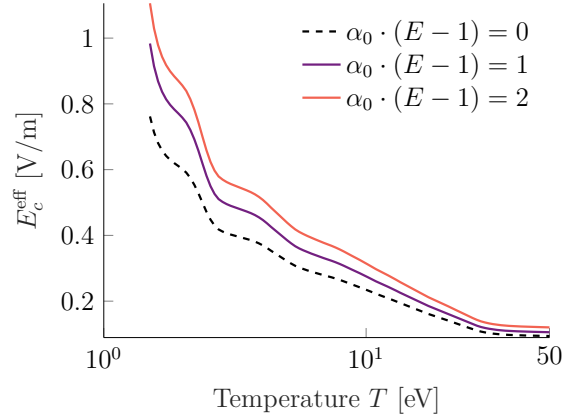
Figure 4.7: The effective critical electric field as a function of temperature for a plasma consisting of deuterium, $n_{\mathrm{D}} = 10^{20} \mathrm{m}^{-3}$, and argon, $n_{\mathrm{Ar}} = 0.3 \cdot 10^{20} \mathrm{m}^{-3}$, in thermal equilibrium as described in section 4.2. The diffusion constant is of the form (3.23) where $\alpha_0 \cdot (E-1)$ quantifies the diffusion strength. Most of the dependence on the critical electric field is inherited from the purely radiative theory (dashed line) and the effective critical field in the presence of diffusion is larger but the offset varies with temperature.

To describe the effect of diffusion in a more complete picture on reactor scales, it is often needed to allow for a spatial variation of the electric field. To this end, we will in the following chapter investigate a perturbation approach to incorporate the effect of gradients in the electric field on the growth rate in the presence of diffusion. This approach will result in integral equations of a similar form to the ones already considered, such that the same numerical solvers can be used.

5

Growth rate corrections in the presence of electric field gradients

Under normal operation of a tokamak there are radial gradients in the temperature and plasma current, both of which contribute to a radially varying electric field as the plasma is drastically cooled in a disruption. The subsequent evolution of the electric field is described by the inductive equation (2.24) which for a cylindrical plasma with only radial variations is [29]

$$\mu_0 \frac{\partial j_{||}}{\partial t} = \frac{1}{r}\frac{\partial}{\partial r} r \frac{\partial E}{\partial r}.\tag{5.1}$$

Therefore the time evolution of the electric field is dependent on its radial profile, as the current $j_{||}$ has both an ohmic and a runaway component. Accordingly the radial profile of runaway generation also plays a crucial part for understanding the electric field evolution. Furthermore, the growth rate is proportional to the electric field strength, for fields large compared to the critical one, such that the cumulative generation is highly dependent on the evolution of the electric field. Consequently, for a self-consistent treatment of both the electric field dynamics and runaway generation, it is of the utmost importance to be able to treat the runaway generation in a region of space with an electric field gradient.

5.1 A perturbative approach to a local theory

The approach to solve the kinetic equation in the high energy region with a momentum space dependent diffusion coefficient in sections 3.1 and 3.2, by the means of a Bessel mode expansion, breaks down when a radial dependence is introduced in the plasma parameters[1] (electric field, diffusion coefficient, density and temperature). To investigate the effects of these gradients we will take a perturbative approach to solving the kinetic equation (3.10) under a quasi-steady-state assumption,

$$x(r)F + \frac{\partial}{\partial p}\left(\frac{U(r,p)}{E(r)-1}F\right) = \frac{\tau}{E(r)-1}\frac{1}{r}\frac{\partial}{\partial r}r\langle D\rangle_\xi(r,p)\frac{\partial F}{\partial r}\tag{5.2}$$

---

[1]The limiting factor is gradients in the electric field or density. With only radial gradients in the diffusion coefficients, the radial part of the problem can still be formulated as a Sturm-Liouville problem which would generate a basis set other than than Bessel modes for the radial profiles. In practice though, such an approach might not be suitable as the basis set would have to be identified for every radially dependent diffusion coefficient.

where the right hand side of the equation is considered to be small. This is expected to be especially valid for strong electric fields or weak diffusion coefficients. Rather than a linear perturbation theory in F we will expand $g = \ln\left(\frac{U}{E-1}F\right)$ as motivated by the solution without radial gradients. In terms of g, the kinetic equation (5.2) is

$$
x(r) + \frac{U}{E-1}\frac{\partial g}{\partial r} = \frac{\tau U}{(E-1)^2}\left[\frac{1}{r}\frac{\partial}{\partial r}r\langle D\rangle_\xi\left(\frac{\partial}{\partial r}\left(\frac{E-1}{U}\right) + \frac{E-1}{U}\frac{\partial g}{\partial r}\right)\right.
$$
$$
\left. + \langle D\rangle_\xi\left(\frac{\partial}{\partial r}\left(\frac{E-1}{U}\right) + \frac{E-1}{U}\frac{\partial g}{\partial r}\right)\frac{\partial g}{\partial r}\right].
$$
(5.3)

and an expansion of the form $g = g_0 + g_1 + \dots$ and $x = x_0 + x_1 + \dots$ results in a first order equation

$$
x_0 + \frac{U}{E-1}\frac{\partial g_0}{\partial p} = 0.
$$
(5.4)

This equation is solved by the method of integrating factor and the low energy boundary condition is formulated as the flow of runaway electrons from a low energy region into the high energy region, as presented in section 3.2. For the first order solution an explicit solution of the boundary condition results in $x_0 = x_r$ and the growth rate is the uncorrected one, as the effect of spatial diffusion is a higher order effect. The corresponding distribution function of the lowest order solution is

$$
F_0(r,p) = \frac{E-1}{U(r,p)}e^{g_0} = n_{\mathrm{RE}}\frac{\gamma_r\tau}{U(r,p)}e^{-x_r\int_{p*}^p dp'\,\frac{E-1}{U(r,p')}},
$$
(5.5)

based on which we define the local equivalents to k^2 and α as

$$
\alpha(r,p) = \frac{\tau\langle D\rangle_\xi}{E-1}k^2(r,p)
$$
(5.6a)

$$
k^2(r,p) = -\frac{F_0^{-1}}{\langle D\rangle_\xi}\frac{1}{r}\frac{\partial}{\partial r}r\langle D\rangle_\xi\frac{\partial F_0}{\partial r}.
$$
(5.6b)

It will be later seen that α characterises the local diffusion strength. With a runaway electron density n_{RE} proportional to a single Bessel mode in a plasma with constant plasma parameters, these "local" definitions reduces to the ones provided in chapter 3. In terms of α the second order contribution to equation (5.3) is

$$
x_1 + \frac{U}{E-1}\frac{\partial g_1}{\partial p} = -\alpha(r,p)
$$
(5.7)

which once again can be solved in a similar manner to the first order equation (5.4), resulting in a combined distribution function of the form

$$
\tilde{F}(r,p) = \frac{E-1}{U(r,p)}e^{g_0+g_1} = n_{\mathrm{RE}}\frac{\gamma_r\tau}{U(r,p)}C(r)e^{-\int_{p*}^p dp'\,\frac{E-1}{U(r,p')}(\tilde{x}+\alpha)}
$$
(5.8)

with $\tilde{x} = x_0 + x_1$ and $C(r)$ a constant of integration. The momentum space dependence of the distribution function is similar to the one for a single Bessel mode

in (3.13) and application of the boundary condition therefore results in the same type of equation for the growth rate as (3.19b). A conceptual difference is that $\tilde{x}$ is now defined locally at every radial position, rather than on the discrete index of the Bessel modes. As the growth rate correction is formulated with the same type of equation found in chapter 3, it is possible to use the same numerical solvers presented in chapter 4 to solve the integral equations. However, there is an extra computational cost to evolve the runaway profile in time, as it typically takes more radial grid points to describe a realistic profile well than it does to describe it with Bessel modes.

By definition of the runaway density n_{RE} as the momentum space integral of F in the high energy region, the constant $C(r)$ is set to unity, which fixes the solution for a given radial profile of runaway electrons. Such a radial profile could be taken from a fluid plasma simulation. The idea would thus be to use the fluid simulation code to evolve the plasma state in time and use the corrected growth rate as a source term for the runaway electron density.

Within this formulation, α is not necessarily positive and the corrected growth rate is therefore not necessarily smaller than γ_r, a manifestation that a net amount of particles can be transported into a region. The remaining part of this thesis will be concerned with investigating the validity and consequences of such local theories.

5.2 Validation of the local theory

The perturbative approach which is detailed in section 5.1 concludes in a distribution function (5.8) which is the solution to a kinetic equation of the form

$$xF + \frac{\partial}{\partial p}\left(\frac{U}{E-1}F\right) = -\alpha(r,p)F \tag{5.9}$$

where α is defined based on the quasi steady-state solution to the kinetic equation F_0 where the influence of the transport has been neglected. This equation is not in a conservative form, with the potential for anomalous particle losses. To quantify this effect, the right hand side of equation (5.9) is integrated over the two dimensional phase space to obtain the loss of the total number of runaway electrons, $n_{tot} = 2\pi \int_0^a dr\, r n_{\mathrm{RE}}$, as

$$\left.\frac{\partial n_{tot}}{\partial t}\right|_{\mathrm{loss}} = \int_{p_*}^{p_{\max}} dp \left[\underbrace{2\pi a\, D(a,p)\left.\frac{\partial F_0}{\partial r}\right|_a \frac{F}{F_0}}_{\sim\,\text{Flux through wall}} - \underbrace{\int_0^a dr\, 2\pi r\, D(r,p)\frac{\partial F_0}{\partial r}\frac{\partial}{\partial r}\left(\frac{F}{F_0}\right)}_{\text{Anomalous particle loss}} \right] \tag{5.10}$$

where integration by parts has been performed. The first term in the equation above can be interpreted as the flux through the wall which almost has the expected form of a diffusive process. The difference is that the flux is related to the gradient of the first order solution - a natural consequence of the fact that it is the first order solution which appears in the diffusion operator. The second term in the equation

is the anomalous part, which should vanish in the no diffusion limit as $F \to F_0$. In the remaining part of this section we will investigate the impact of this anomalous loss, and the validity of the perturbation expansion in general.

5.2.1 Without electric field gradients

A first test for the local version of the theory is to compare it to the theory described in sections 3.1 and 3.2, in situations where these calculations are valid. It should be noted that the two theories do not solve exactly the same equation, as the quasi steady-state approximation is made at different points in the derivation. In situations where the mode theory of chapter 3 is valid there is no motivation to use the local theory, as it introduces extra approximations, is not guaranteed to be conserve particles and is more computationally expensive (as was described in the end of section 5.1).

Without radial gradients in the plasma parameters, the local definition of α, equation (5.6), reduces to

$$\alpha(r, p) = -\frac{\tau D(p)}{E - 1} n_{\mathrm{RE}}^{-1} \frac{1}{r} \frac{\partial}{\partial r} r \frac{\partial n_{\mathrm{RE}}}{\partial r} \tag{5.11}$$

and only depends on the spatial gradients of the runaway electrons density. This local diffusion strength results in a spatially dependent generation rate of runaway electrons, $\gamma(r) n_{\mathrm{RE}}$, where $\gamma(r)$ is determined by (3.21) and $\alpha(r, p)$. Likewise, in the Bessel mode formulation, the time evolution of the runaway profile is

$$n_{\mathrm{RE}}(r, t) = \sum_{i=1}^{\infty} c_i e^{\gamma_i t} J_0 \left(b_i r / a \right) \tag{5.12}$$

where J_0 is the zeroth Bessel function, b_i its zeros, c_i is a set of projection coefficients and γ_i is the corrected growth rate for the i-th Bessel mode obtained from (3.21). Thus the local rate of runaway electron generation in the mode based theory is

$$\frac{\partial n_{\mathrm{RE}}}{\partial t} = \sum_{i=1}^{\infty} \gamma_i c_i e^{\gamma_i t} J_0(k_i r) \tag{5.13}$$

which is more easily compared to the local theory than the corrected growth rates for the individual Bessel modes.

Two examples of the differences between the Bessel mode expansion and the local theory can be seen in figure 5.1. Good agreement is observed in the case where diffusion causes only a small correction and the perturbation approach is expected to be valid. In figure 5.1b the growth is significantly altered by the diffusion, yet although some discrepancies are seen between the local and the mode theory, the local approximation is still much closer than the uncorrected theory.

The anomalous losses are small in the tests showcased in figure 5.1, more precisely the total anomalous losses are 0.1% and 1.7% of the total generation of runaway electrons for 5.1a and 5.1b respectively. The anomalous losses should be compared
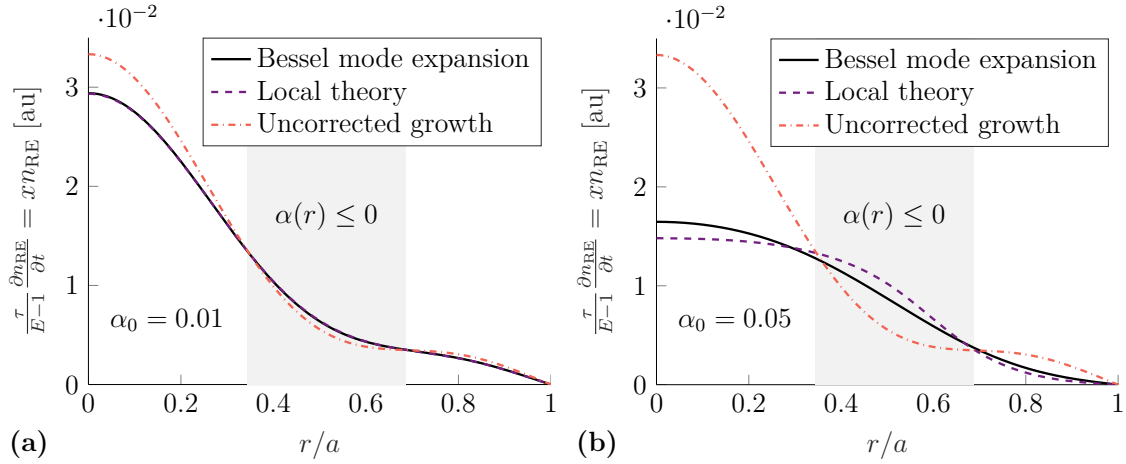
Figure 5.1: Radial profiles of the runaway growth given by the local theory (dashed line) and the Bessel mode expansion (solid line). We allow for a diffusion coefficient of the form $(1 + p^2)^{-1/2}$, equation (3.23), and a normalised diffusion strength equal to: (a) $\alpha_0 = 0.01$ and (b) $\alpha_0 = 0.05$ for the first Bessel mode. To model radiation a large-p expansion has been used for the acceleration function $U(p)$ and a constant electric field strength $E = 1.5$, close to the critical value in the purely radiative theory of $E_c^{\text{eff, rad}} \approx 1.28$, is used. The plasma parameters are $Z_{\text{eff}} = 1$, $\ln \Lambda = 15$ and the uncorrected growth rate was chosen to be $x_r = (2 \ln \Lambda)^{-1}$. Good agreement between the models is seen in the case where the correction to the growth rate is small, however a larger discrepancy is observed for the larger diffusion case. The local theory is still substantially closer to the correct result than the uncorrected one (dashed-dotted line). The initial runaway electron profile is proportional to the uncorrected growth, as the uncorrected growth is $x_r n_{\text{RE}}$.
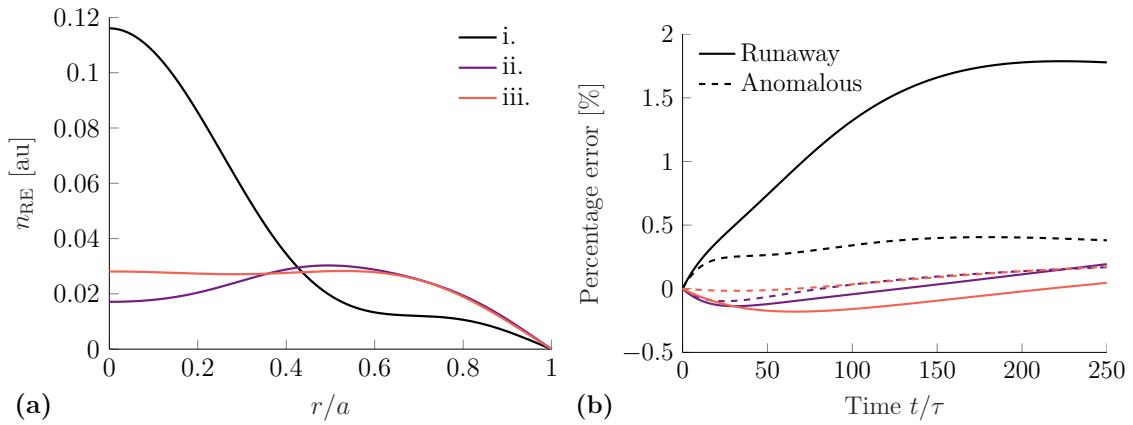
Figure 5.2: (a) Initial profiles of the runaway current, all normalised to have the same total number of runaways. (b) Percentage error for the local theory in the total runaway current, after the profiles in (a) have been evolved in time with a combination of avalanche generation and diffusion without electric field gradients. The dashed lines correspond to the time integration of the anomalous term, shown in equation (5.10). The error is seen in the initial phase to be dominated by the anomalous term, but in the later stages the combined effect of transport errors and previous losses of particles due to the anomalous term, result in an altered growth. A constant percentage error would correspond to two profiles with the same growth rate but slightly different particle number. The plasma parameters, diffusion model and electric fields are all the same as in figure 5.1b.

to the flux through the wall which are about 2.6% and 11% for the two cases. As expected the anomalous part is seen to be small when the perturbative expansion is valid.

Figure 5.2b shows the cumulative error when the initial runaway profiles shown in 5.2a are evolved in time with the mode theory and the local theory. In the initial phase of the evolution, the error is seen to correspond to the anomalous flux given in equation (5.10), but in the later stages the error from not capturing the transport fully (as is seen in 5.1b) combined with the previous anomalous error result in slightly different profiles and consequently different growth. For the range of profiles tested in figure 5.2a, the percentage error stays below 2%, which includes the worst of the two cases demonstrated in figure 5.1. The anomalous term is seen to both add and subtract particles, depending on the profile of the runaway electron density in question.

The error from the anomalous term in the local theory can easily be traced, by considering the flux of particles into the wall and the total generation of runaway electrons, but the implications of these particle losses as well as non-perfect replication of the transport on the continued evolution is harder to estimate, as an altered profile evolves differently. Furthermore, transport with spatially constant diffusion coefficients has the tendency to reduce gradients in the runaway profile, in which case the approximation is expected to be more valid. The validity of the approxi-

mation during the whole evolution is thus a question of whether the generation of runaway electrons is localised enough to generate strong gradients in the runaway density.

For the time propagation of the runaway electron profiles, an explicit time step based on the corrected growth rate is prone to instabilities due to the characteristic exponential growth. Therefore an implicit scheme was implemented based on a predictor-corrector method, functionally equivalent to solving a linearised system of equations in every correction step. The full procedure of such an implementation is described in appendix A.1.

5.2.2 With electric field gradients

To further test the local theory, now in non-uniform electric fields where the Bessel expansion breaks down, a PDE-solver was implemented for equation (3.4) which is the original kinetic equation from which the integral theory for the non-radiative model was derived. The PDE solver is based on a finite difference approach and is fully implicit - the details of which are described in appendix A.2.

When all plasma parameters are constant, and radiation as well as screening effects are neglected (such that x_r is constant), α still takes the form of (5.11). Therefore the implicit time propagation algorithm presented in appendix A.1 can also be used, in the non-radiative limit, to compare the local theory to the PDE solver for equation (3.4). In figures 5.3 and 5.4 two different cases with different initial runaway distributions and electric field structures can be seen. Overall good agreement is seen between the models, although the very strong diffusion cases could not be tested, as the integral equation (3.7) does not have a solution for diffusion coefficients decaying as p^{-1} or faster for large momenta. This is related to the discussion of convergence in section 3.3.

The final runaway electron profiles from the PDE-solver with a distribution function initiated according to (5.8) and with a time propagation according to the local theory, agree well after having evolved for 30τ, as is shown in figures 5.3a and 5.4a, where two significantly different electric field structures have been used. This shows that the local theory can capture a change in the density profile caused by the combined effect of diffusion and a spatially varying avalanche generation. Quantitatively the total number of runaways differ between the two solutions by 1.6% and 2.1% for the two different cases, which is comparatively small compared to the total effect of diffusion, which reduces the total runaway current by about 35% in both cases.

Despite good agreement in the density between the two methods for time propagation, some differences can be seen in the momentum space distribution functions. The difference is especially pronounced at high momenta, but the small number of particles at these energies results in a quite small impact on the total number of particles at a radial position. The main reason this occurs is that in the integral theory the whole momentum space distribution is dependent on the growth rate x, thus
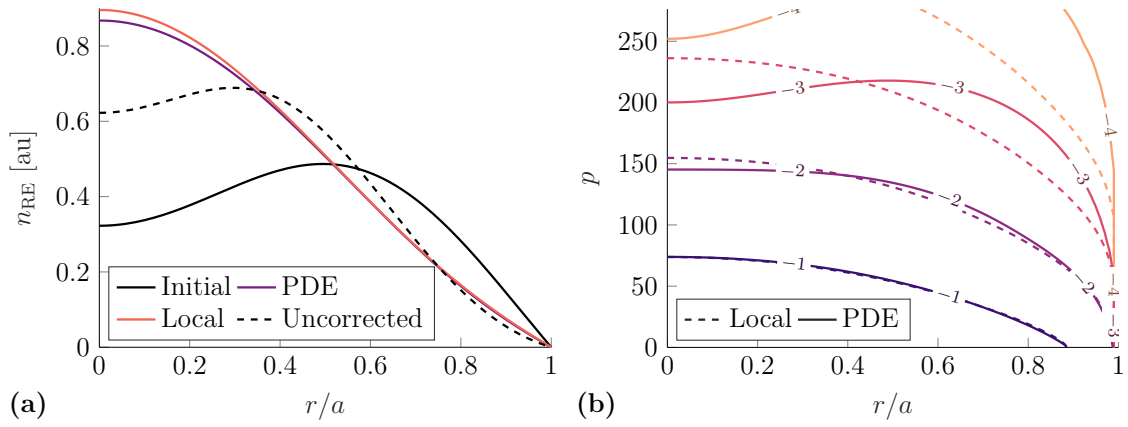
Figure 5.3: (a) Normalised profiles of the runaway density. The initial profile (initial) is propagated in time by 30τ both according to the local theory (local) and with the PDE solver (PDE) in a non-uniform electric field where the electric field strength is $E = 5 - 2\left(r/a\right)^2$ in units of E_c. For reference the profile is propagated for the same length of time without effects of diffusion (uncorrected). All profiles are normalised to have the same amount of particles except (local) which has been normalised with the same factor as (PDE). A spatially constant diffusion constant is employed with $D_0\tau/a^2 = 0.022$ with a decaying strength in momentum space according to (3.23). The normalised growth rate is $x_r = \left(2\ln\Lambda\right)^{-1}$ and $\ln\Lambda = 15$. (b) Contours of $\log_{10} F$ of the two dimensional distribution function of the profiles (local) and (PDE) in figure 5.3a. For the PDE solution the distribution function is obtained from the numerical solver and for the local theory the distribution function is according to (5.8). The solutions are shown to agree well for low momenta.
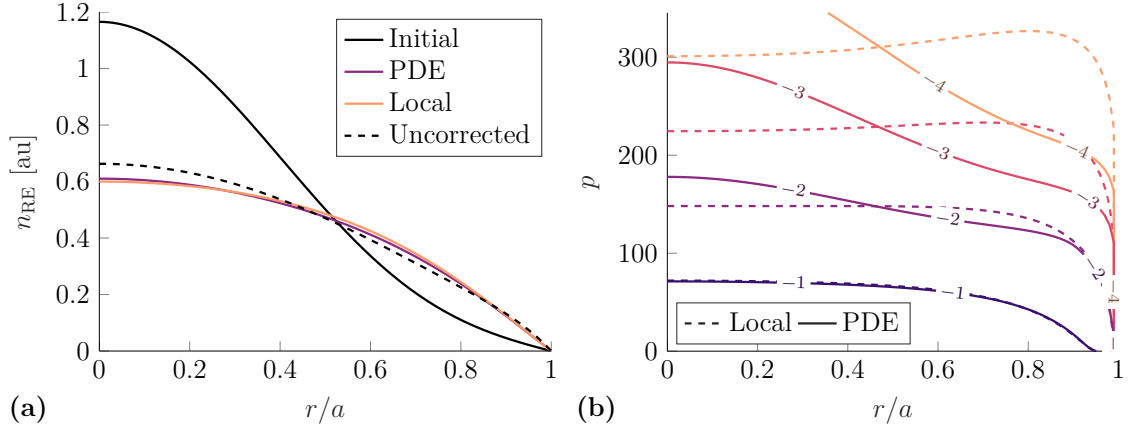

Figure 5.4: (a) Normalised profiles of the runaway density. The seed population (initial) is propagated for 30τ both according to the local theory (local) and with a PDE solver (PDE). A non-constant electric field with a minimum on axis is used, of the form $E = 3 + 2\left(r/a\right)^2$ in units of E_c. Plasma parameters and diffusion coefficients are otherwise the same as in figure 5.3a. (b) Two dimensional plot of $\log_{10} F$ for the profiles (local) and (PDE) in figure 5.4a. The solutions are shown to agree well closer to the lower limit of the high energy region where the avalanche electrons flow in and where the diffusion is stronger.

changes to the runaway density profile propagate through all of momentum space, but in the PDE solution particles are transported according to the diffusion operator which then takes time to alter the profiles, especially at large energies where the diffusion is weak. The momentum space structure is seen to agree to a larger extent if the simulation is run for a longer time, as the shape of the runaway density profile is stabilising and time variations in the growth rate are not accounted for in the quasi-steady state approximation.

The discrepancies in the very high energy populations of runaway electrons do not affect the macroscopic quantities, such as the runaway density and corresponding current, as demonstrated above. However a common way to investigate the runaway beam after a disruption is by the emitted spectrum of synchrotron radiation [80–82]. The contribution of the high energy electrons to such a spectrum is dominant. Therefore the synchrotron measurements predicted by the two models might not agree to the same extent as the measurements of the current. It should be noted that the results in this section do not include radiation effects. The inclusion of radiation reaction forces limits the maximum energy of the runaway electrons to a region with a stronger diffusion, which might give a better agreement at high momentum. This effect, as well as the effect of gradients in all plasma parameters, needs to be investigated further to validate the theory.

6
Conclusion

Tokamaks are today the leading contender to achieve fusion energy production on a commercial scale, but the large plasma current they carry has the potential to be converted to a high energy beam of runaway electrons during disruptions. Such a beam poses a serious threat to plasma-facing components and the reliable operation of reactor scale tokamaks. Therefore it is of the highest priority to predict and avoid disruptions. However, it must be accepted that a perfect success rate in preventing disruptions may be unrealistic and mitigating any damage when they occur is crucial. The disruption mitigation system for the ITER tokamak is currently under development, a process in need of accurate models of the runaway phenomenon. Runaway electrons travel rapidly along the tokamak magnetic field lines, and these can be severely distorted from their usual confining structure during disruptions. In this thesis, we have presented a model to include the effects of radial transport due to the interaction of runaway electrons with magnetic field perturbations on the runaway dynamics. In particular, we have determined an expression which can be used to correct the growth rate of the runaway electron population by the avalanche mechanism. The perturbations can mitigate the effects of runaway electrons as the resulting transport has the opportunity to remove them in a controlled manner, before they have had the time to multiply through the avalanche mechanism.

Summary

Starting from the kinetic equation we take advantage of the separation of timescales in runaway generation between the acceleration to relativistic energies after a knock-on collision, and the characteristic avalanche population growth time. This allows us to neglect the effect of transport due to magnetic perturbations on the generation process and focus on solving the kinetic equation in the high energy limit, which simplifies the collision operator. The description of collisions accounts for effects of partial screening through the expressions of the collision frequency, therefore such effect is naturally included here. We then use the fact that close to the point where the radiation reaction forces balance the electric field acceleration, pitch angle scattering is rapid compared to the energy dynamics and general expressions for the pitch angle dependence of the distribution in the high energy region can be established. This approximation is valid when the effects of radiation are expected to be important, and as the dynamics at energies significantly below the balancing point is dominated by the electric field. The acceleration due to the electric field is not strongly dependent on the pitch angle distribution as long as the electron beam is forward focused, which the runaway distribution is expected to be. Finally,

upon pitch-angle averaging a general operator representing radial diffusion, we obtain the expression for the growth rate during the avalanche, which takes the form of the solution of an integral equation. This extends previous work on the effects of perturbations on runaway evolution where radiation and screening effects were neglected as well as the effect of the pitch angle distribution on the transport, as the theory was an expansion around small pitch angles. Furthermore, the previous treatment was primarily concerned with transport coefficients with a short range in momentum space, while here transport coefficients with a long range in momentum space were mainly of interest. The introduction of radiation is expected to impact the theory as it introduces an upper limit in momentum space and the particles are prevented from reaching very high energies where they are well confined.

The radial transport was considered to be diffusive, which is expected when the transport originates from perturbations in the magnetic field. We have investigated simple momentum space forms of the diffusion coefficients, which nonetheless are motivated by the expected behaviour, as they allowed closed form solutions to be developed in order to understand the impact of perturbations and provide benchmarking cases. An explicit approximation in the weak diffusion limit or equivalently in the strong electric field limit for the corrected avalanche growth rate was also obtained.

A numerical method was developed, able to solve for the corrected growth rate for an arbitrary diffusion coefficient. This allowed the study of diffusion coefficients based on forms existing in the literature, which account for the spread of electron velocities parallel to the magnetic field, and finite orbit width effects in stochastic field regions which typically will have finite correlation length-scales. The more complete description of the effect of perturbations leads to a weaker diffusion at low velocities. We find that this essentially removes the dependence of the result on the choice of high energy region, denoted by a cutoff in momentum space p_*, when large electric fields are considered.

The robustness of the numerical scheme developed to evaluate the corrected growth is an important attribute and a novel combination of well-known algorithms was used to achieve this. The robustness was especially important as we anticipate that the solver can act as a subroutine within a larger framework used to model disruptions. The explicit expressions for correcting the growth rate could be used in the modelling of disruptions, essentially without adding any computational cost, when investigating the plateau phase and the large electric field regime. Otherwise, the full numerical solver allows screening and spatial diffusion to be accounted for self-consistently in disruption modelling. To account for gradients in the plasma parameters, such as electric field and electron density, a local version of the theory was found by a perturbation expansion in weak diffusion strengths. Some initial tests of a local version of the theory were carried out, and the predictions of such a theory were compared to the solution of a PDE-solver. The initial results are promising although further investigations are needed.

The diffusive transport raises the effective critical electric field for avalanche generation because even though particles can be kicked into the runaway region through the avalanche mechanism, they can be lost due to spatial diffusion resulting in no net gain of runaways. This is important for the dynamics in the plateau phase of disruptions where the electric field tends to a value at which the loss and gain of runaway electrons is balanced. The critical electric field behaviour was studied in more detail with a second similar numerical solver. The critical electric field is seen to match the purely radiative theory in the limit of no diffusion and an almost linear relation between the diffusion strength and the critical electric field is found. Consequently, the correction of the critical electric field is predicted to scale as $\sim (\delta B/B)^2 / L^2$ where $\delta B/B$ is the fractional perturbation of the magnetic field and L the characteristic radial length scale of the runaway population. Note that the correction is not predicted to scale with plasma density in physical units, whereas the uncorrected critical field is directly proportional to the density.

Further work

With the model and numerical solver developed above, we have the potential to explore a range of effects on runaway electron dynamics. The fusion community is working to further develop transport models appropriate for runaway electrons and determine in which scenarios they are valid. This requires a better understanding of the magnetic field structure during time evolving situations such as disruptions, which could be obtained by MHD-simulations. In principle, this process should be carried out in conjunction with an evolving profile of runaway electrons to self-consistently follow the evolution of the electric and magnetic fields. The evaluation of transport coefficients in non-stochastic fields will probably require the use of particle following codes, which follow the trajectories of test particles in the perturbed field and fit a diffusive-advective transport model, as was done in [72].

A kinetic effect lacking in the model we have presented is the impact of diffusion on the avalanche generation mechanics at momentum scales close to the critical one. We anticipated that this effect could be small compared to the effects investigated so far, as the runaway electrons spend a comparatively short amount of time close to the critical momentum. Analytical progress in this direction would require the addition of a radial dimension in the full kinetic calculation with the source term in Refs. [23, 51] to treat the dynamics close to the critical momentum, then the development of a solution to the kinetic equation valid for large momenta in the same calculation. Numerical progress, on the other hand, could be made directly by implementing the diffusion operator in kinetic frameworks such as CODE [83, 84], which determine the electron distribution function as the solution to the kinetic equation, using suitable models for the collision operator. Such an implementation would further provide knowledge on the pitch angle distribution and especially the influence of a pitch angle dependent diffusion coefficient on the pitch-angle distribution, an effect which has not been considered in the present work.

Finally, to acquire a better understanding of the influence of the runaway electron transport on reactor scales during a disruption, the model presented in this thesis could be used, as noted above, in a disruption framework to evolve the runaway profile, together with the rest of the plasma parameters, most notably the electric field. Such computations could be carried out with the GO-framework [29, 85–87] or similar ones. The GO-framework uses a (multi-) fluid model for the evolution of a disruptive plasma. Introducing the effect of transport into such a model of the system, including the effects of impurities and allowing for partial screening, would allow us to finally quantify the reduction transport has on the total number of runaway electrons at the end of disruptions. As runaway electrons need to be avoided to protect the integrity of the inner wall, a still open relevant question is whether a given transport coefficient would result in a tolerable energy flux on the inner wall. The runaway electrons would still hit the surrounding structure, but in a more controlled manner than if the control is lost of a fully formed runaway beam. For such considerations, it would probably be necessary to have a more complete picture of the disruption evolution, which could be provided by numerical investigations of fluid models.

Bibliography

[1]   D. A. Gurnett and A. Bhattacharjee, *Introduction to plasma physics: with space and laboratory applications* (Cambridge University Press, 2005).

[2]   A. Gurevich, G. Milikh, and R. Roussel-Dupre, "Runaway electron mechanism of air breakdown and preconditioning during a thunderstorm", Physics Letters A **165**, 463–468 (1992).

[3]   C. F. Kennel, "Consequences of a magnetospheric plasma", Reviews of Geophysics **7**, 379–419 (1969).

[4]   J. F. Waymouth and F. Bitter, "Analysis of the plasma of fluorescent lamps", Journal of Applied Physics **27**, 122–131 (1956).

[5]   E. G. Gamaly, *Femtosecond laser-matter interaction: theory, experiments and applications* (CRC Press, 2011).

[6]   J. Wesson and D. J. Campbell, *Tokamaks*, Vol. 149 (Oxford University Press, 2011).

[7]   J. E. Lennard-Jones, "On the determination of molecular fields.—II. from the equation of state of a gas", Proceedings of the Royal Society of London. Series A, Containing Papers of a Mathematical and Physical Character **106**, 463–477 (1924).

[8]   J. O'Toole and J. Dahler, "Molecular friction in dilute gases", The Journal of Chemical Physics **33**, 1496–1504 (1960).

[9]   S. Chandrasekhar, "Dynamical friction. I. general considerations: the coefficient of dynamical friction.", The Astrophysical Journal **97**, 255 (1943).

[10] F. L. Hinton, "Collisional transport in plasma", Handbook of Plasma Physics **1**, 147 (1983).

[11] F. Andersson, P. Helander, and L.-G. Eriksson, "Damping of relativistic electron beams by synchrotron radiation", Physics of Plasmas **8**, 5221–5229 (2001).

[12] E. Hirvijoki, I. Pusztai, J. Decker, O. Embréus, A. Stahl, and T. Fülöp, "Radiation reaction induced non-monotonic features in runaway electron distributions", Journal of Plasma Physics **81**, 475810502 (2015).

[13] A. Rechester and M. Rosenbluth, "Electron heat transport in a tokamak with destroyed magnetic surfaces", Physical Review Letters **40**, 38 (1978).

[14] P. Helander, L.-G. Eriksson, and F. Andersson, "Suppression of runaway electron avalanches by radial diffusion", Physics of Plasmas **7**, 4106–4111 (2000).

[15] D. MacKay, *Sustainable energy-without the hot air* (UIT Cambridge, 2008).

[16] G. Gamow, "Zur quantentheorie des atomkernes", Zeitschrift für Physik **51**, 204–212 (1928).

[17] R. Atkinson and F. G. Houtermans, "Zur Frage der Aufbaumöglichkeit der Elemente in Sternen", Zeitschrift für Physik **54**, 656–665 (1929).

[18] A. Eddington, "On the radiative equilibrium of the stars", Monthly Notices of the Royal Astronomical Society **77**, 16–35 (1916).

[19] L. Spitzer Jr, *A proposed stellarator*, tech. rep. (Princeton Univ., NJ Forrestal Research Center, 1951).

[20] F. Chen et al., *Introduction to plasma physics and controlled fusion*, Vol. 1 (Springer, 1984).

[21] T. Hender, J. Wesley, J. Bialek, A. Bondeson, A. Boozer, R. Buttery, A. Garofalo, T. Goodman, R. Granetz, Y. Gribov, et al., "MHD stability, operational limits and disruptions", Nuclear fusion **47**, S128 (2007).

[22] L. Spitzer Jr and R. Härm, "Transport phenomena in a completely ionized gas", Physical Review **89**, 977 (1953).

[23] M. Rosenbluth and S. Putvinski, "Theory for avalanche of runaway electrons in tokamaks", Nuclear Fusion **37**, 1355 (1997).

[24] B. N. Breizman, P. Aleynikov, E. M. Hollmann, and M. Lehnen, "Physics of runaway electrons in tokamaks", Nuclear Fusion **59**, 083001 (2019).

[25] E. M. Hollmann, P. B. Aleynikov, T. Fülöp, D. A. Humphreys, V. A. Izzo, M. Lehnen, V. E. Lukash, G. Papp, G. Pautasso, F. Saint-Laurent, and J. A. Snipes, "Status of research toward the ITER disruption mitigation system", Physics of Plasmas **22**, 021802 (2015).

[26] L. Hesslow, O. Embréus, O. Vallhagen, and T. Fülöp, "Influence of massive material injection on avalanche runaway generation during tokamak disruptions", Nuclear Fusion **59**, 084004 (2019).

[27] *ITER - the way to new energy*, https://www.iter.org.

[28] A. H. Boozer, "Theory of runaway electrons in ITER: Equations, important parameters, and implications for mitigation", Physics of Plasmas **22**, 032504 (2015).

[29] H. Smith, P. Helander, L.-G. Eriksson, D. Anderson, M. Lisak, and F. Andersson, "Runaway electrons and the evolution of the plasma current in tokamak disruptions", Physics of Plasmas **13**, 102502 (2006).

[30] P. Debye and E. Hückel, "The theory of electrolytes: I. lowering of freezing point and related phenomena", Phys. Z **24**, 1 (1923).

[31] A. A. Vlasov, "The vibrational properties of an electron gas", Soviet Physics Uspekhi **10**, 721–733 (1968).

[32] R. D. Hazeltine and J. D. Meiss, *Plasma confinement* (Courier Corporation, 2003).

[33] H. Alfvén, "Existence of electromagnetic-hydrodynamic waves", Nature **150**, 405–406 (1942).

[34] K. H. Spatschek, "Reduced descriptions for complex plasmas: Simple examples, plasma kinetics, and transport truncations", Fusion Science and Technology **45**, 135–150 (2004).

[35] P. Helander and D. J. Sigmar, *Collisional transport in magnetized plasmas*, Vol. 4 (Cambridge University Press, 2005).

[36] H. Dreicer, "Electron and ion runaway in a fully ionized gas. I", Physical Review **115**, 238 (1959).

[37] H. Dreicer, "Electron and ion runaway in a fully ionized gas. II", Physical Review **117**, 329 (1960).

[38] L. Hesslow, "Effect of partial screening on runaway-electron dynamics", Licentiate thesis (Chalmers University of Technology, 2018).

[39] L. Hesslow, O. Embréus, G. J. Wilkie, G. Papp, and T. Fülöp, "Effect of partially ionized impurities and radiation on the effective critical electric field for runaway generation", Plasma Physics and Controlled Fusion **60**, 074010 (2018).

[40] J. Connor and R. Hastie, "Relativistic limitations on runaway electrons", Nuclear fusion **15**, 415 (1975).

[41] L. Hesslow, O. Embréus, A. Stahl, T. C. DuBois, G. Papp, S. L. Newton, and T. Fülöp, "Effect of partially screened nuclei on fast-electron dynamics", Physical Review Letters **118**, 255001 (2017).

[42] L. Hesslow, O. Embréus, M. Hoppe, T. C. DuBois, G. Papp, M. Rahm, and T. Fülöp, "Generalized collision operator for fast electrons interacting with partially ionized impurities", Journal of Plasma Physics **84**, 905840605 (2018).

[43] W. Rindler, *Relativity: special, general, and cosmological* (American Association of Physics Teachers, 2003).

[44] E. Hirvijoki, J. Decker, A. Brizard, and O. Embréus, "Guiding-centre transformation of the radiation–reaction force in a non-uniform magnetic field", Journal of Plasma Physics **81**, 475810504 (2015).

[45] O. Embréus, A. Stahl, and T. Fülöp, "Effect of bremsstrahlung radiation emission on fast electrons in plasmas", New Journal of Physics **18**, 093023 (2016).

[46] C. T. R. Wilson, "The electric field of a thundercloud and some of its effects", Proceedings of the Physical Society of London **37**, 32D (1924).

[47] C. T. R. Wilson, "The acceleration of β-particles in strong electric fields such as those of thunderclouds", in Mathematical Proceedings of the Cambridge Philosophical Society, Vol. 22, 4 (Cambridge University Press, 1925), pp. 534–538.

[48] A. Eddington, *The internal constitution of stars* (Cambridge University Press, 1826).

[49] M. D. Kruskal and I. B. Bernstein, "Runaway electrons in an ideal Lorentz plasma", The Physics of Fluids **7**, 407–418 (1964).

[50] I. Sokolov, "Multiplication' of accelerated electrons in a tokamak", JETP Letters **29**, 218–221 (1979).

[51] R. Jayakumar, H. Fleischmann, and S. Zweben, "Collisional avalanche exponentiation of runaway electrons in electrified plasmas", Physics Letters A **172**, 447–451 (1993).

[52] A. H. Boozer, "Physics of magnetically confined plasmas", Reviews of Modern Physics **76**, 1071 (2005).

[53] B. V. Chirikov et al., "A universal instability of many-dimensional oscillator systems", Physics Reports **52**, 263–379 (1979).

[54] E. Nardon, "JOREK simulations of MGI-triggered disruptions in JET", in Runaway electron modelling (REM) meeting 8 (2020).

[55] R. Yoshino and S. Tokuda, "Runaway electrons in magnetic turbulence and runaway current termination in tokamak discharges", Nuclear Fusion **40**, 1293 (2000).

[56] M. Lehnen, S. A. Bozhenkov, S. S. Abdullaev, and M. W. Jakubowski (TEXTOR Team), "Suppression of runaway electrons by resonant magnetic perturbations in TEXTOR disruptions", Physical Review Letters **100**, 255003 (2008).

[57] V. Riccardo, G. Arnoux, P. Cahyna, T. Hender, A. Huber, S. Jachmich, V. Kiptily, R. Koslowski, L. Krlin, M. Lehnen, et al., "JET disruption studies in support of ITER", Plasma Physics and Controlled Fusion **52**, 124018 (2010).

[58] G. Papp, M. Drevlak, T. Fülöp, P. Helander, and G. Pokol, "Runaway electron losses caused by resonant magnetic perturbations in ITER", Plasma Physics and Controlled Fusion **53**, 095004 (2011).

[59] G. Papp, M. Drevlak, T. Fülöp, and G. I. Pokol, "The effect of resonant magnetic perturbations on runaway electron transport in ITER", Plasma Physics and Controlled Fusion **54**, 125008 (2012).

[60] M. Rosenbluth, R. Sagdeev, J. Taylor, and G. Zaslavski, "Destruction of magnetic surfaces by magnetic field irregularities", Nuclear Fusion **6**, 297 (1966).

[61] N. Filonenko, R. Sagdeev, and G. Zaslavsky, "Destruction of magnetic surfaces by magnetic field irregularities: part II", Nuclear Fusion **7**, 253 (1967).

[62] T. Hauff and F. Jenko, "Runaway electron transport via tokamak microturbulence", Physics of Plasmas **16**, 102308 (2009).

[63] P. H. Diamond, S. Itoh, and K. Itoh, *Modern plasma physics: Volume 1, Physical kinetics of turbulent plasmas* (Cambridge University Press, 2010).

[64] R. Bickerton, "Magnetic turbulence and the transport of energy and particles in tokamaks", Plasma Physics and Controlled Fusion **39**, 339 (1997).

[65] H. E. Mynick and J. A. Krommes, "Particle diffusion by magnetic perturbations of axisymmetric geometries", Physical Review Letters **43**, 1506 (1979).

[66] J. Myra and P. J. Catto, "Effect of drifts on the diffusion of runaway electrons in tokamak stochastic magnetic fields", Physics of Fluids B **4**, 176–186 (1992).

[67] J. Myra, P. J. Catto, H. Mynick, and R. Duvall, "Quasilinear diffusion in stochastic magnetic fields: reconciliation of drift-orbit modification calculations", Physics of Fluids B **5**, 1160–1163 (1993).

[68]   T. Hauff and F. Jenko, "Turbulent $E \times B$ advection of charged test particles with large gyroradii", Physics of Plasmas **13**, 102309 (2006).

[69]   G. B. Folland, *Fourier analysis and its applications*, Vol. 4 (American Mathematical Soc., 2009).

[70]   P. Aleynikov and B. N. Breizman, "Theory of two threshold fields for relativistic runaway electrons", Physical Review Letters **114**, 155001 (2015).

[71]   N. G. Lehtinen, T. F. Bell, and U. S. Inan, "Monte Carlo simulation of runaway MeV electron breakdown with application to red sprites and terrestrial gamma ray flashes", Journal of Geophysical Research: Space Physics **104**, 24699–24712 (1999).

[72]   K. Särkimäki, E. Hirvijoki, J. Decker, J. Varje, and T. Kurki-Suonio, "An advection–diffusion model for cross-field runaway electron transport in perturbed magnetic fields", Plasma Physics and Controlled Fusion **58**, 125017 (2016).

[73]   G. Engeln-Müllges and F. Uhlig, *Numerical algorithms with C* (Springer Science & Business Media, 2013).

[74]   H. P. Summers, *The ADAS user manual*, 2.6, Atomic Data and Analysis Structure (2014).

[75]   B. N. Breizman, "Marginal stability model for the decay of runaway electron current", Nuclear Fusion **54**, 072002 (2014).

[76]   G. Papp et al., "The effect of high-Z material injection on runaway electron dynamics", in 46th EPS Conference on Plasma Physics (2019).

[77]   S. Galdino, "A family of regula falsi root-finding methods", in Proceedings of the 2011 World Congress on Engineering and Technology (2011).

[78]   N. Anderson and Å. Björck, "A new high order method of regula falsi type for computing a root of an equation", BIT Numerical Mathematics **13**, 253–264 (1973).

[79]   J. Kiefer, "Sequential minimax search for a maximum", Proceedings of the American Mathematical Society **4**, 502–506 (1953).

[80]   K. H. Finken, J. G. Watkins, D. Rusbüldt, W. J. Corbett, K. H. Dippel, D. M. Goebel, and R. A. Moyer, "Observation of infrared synchrotron radiation from tokamak runaway electrons in TEXTOR", Nuclear Fusion **30**, 859 (1990).

[81]   M. Hoppe, O. Embréus, R. Tinguely, R. Granetz, A. Stahl, and T. Fülöp, "SOFT: a synthetic synchrotron diagnostic for runaway electrons", Nuclear Fusion **58**, 026032 (2018).

[82]   M. Hoppe, O. Embréus, C. Paz-Soldan, R. Moyer, and T. Fülöp, "Interpretation of runaway electron synchrotron and bremsstrahlung images", Nuclear Fusion **58**, 082001 (2018).

[83]   M. Landreman, A. Stahl, and T. Fülöp, "Numerical calculation of the runaway electron distribution function and associated synchrotron emission", Computer Physics Communications **185**, 847–855 (2014).

[84] A. Stahl, O. Embréus, G. Papp, M. Landreman, and T. Fülöp, "Kinetic modelling of runaway electrons in dynamic scenarios", Nuclear Fusion **56**, 112009 (2016).

[85] T. Fehér, H. Smith, T. Fülöp, and K. Gál, "Simulation of runaway electron generation during plasma shutdown by impurity injection in ITER", Plasma Physics and Controlled Fusion **53**, 035014 (2011).

[86] G. Papp, T. Fülöp, T. Fehér, P. De Vries, V. Riccardo, C. Reux, M. Lehnen, V. Kiptily, V. Plyusnin, B. Alper, et al., "The effect of ITER-like wall on runaway electron generation in JET", Nuclear Fusion **53**, 123017 (2013).

[87] T. Fülöp, P. Helander, O. Vallhagen, O. Embreus, L. Hesslow, P. Svensson, A. J. Creely, N. T. Howard, and P. Rodriguez-Fernandez, "Effect of plasma elongation on current dynamics during tokamak disruptions", Journal of Plasma Physics **86**, 474860101 (2020).

[88] J. Crank and P. Nicolson, "A practical method for numerical evaluation of solutions of partial differential equations of the heat-conduction type", in Mathematical Proceedings of the Cambridge Philosophical Society, Vol. 43, 1 (Cambridge University Press, 1947), pp. 50–67.

A
Numerical implementation

In chapter 5 two different algorithms are used for propagating the runaway electron profiles in time. The first one is an implicit time step method based on the corrected growth rate from the algorithm presented in section 4.1, which is needed for stability reasons. This algorithm is presented below in A.1. The time propagation based on this algorithm was tested against a second numerical implementation based on a PDE-solver which is presented in A.2. This solver allowed the test of the local theory presented in chapter 5 for non-constant electric fields, carried out in section 5.2.2.

A.1 Implicit time evolution

The numerical algorithm described in chapter 4 can be used to find the local growth rate, $\gamma = \gamma(r)$ in the presence of magnetic perturbations, as described in section 5.1. The naive explicit scheme for evolving the profiles of runaway electrons $n(r,t)$ in time,

$$n(r, t + \delta t) \approx \Big(1 + \gamma\left[n(r,t)\right]\ \delta t\Big)n(r,t) \tag{A.1}$$

where $\gamma\left[n\right]$ is the growth rate based on the profile n, is prone to instabilities. Therefore an implicit scheme is needed. No explicit expression for the growth rate is known for a changing profile, with changing k^2, so a predictor-corrector method was used for the implicit scheme. For the prediction step, equation (A.1) was used, to arrive at the prediction m. The correction step is then based on linearising the equation,

$$n(r, t + \delta t) - n(r,t) = \frac{\delta t}{2}\gamma\left[n(r,t)\right]n(r,t) + \frac{\delta t}{2}\gamma\left[n(r, t + \delta t)\right]n(r, t + \delta t) \tag{A.2}$$

around the prediction $n(r, t + \delta t) = m$ and solving the linear system of equations for the corrected profile n. The correction step is then repeated by using the corrected profile as the prediction. Fortunately, the growth rate is only dependent on k^2 whose discretisation in a point only depends on three neighbouring points, resulting in a tridiagonal system of equations, which can be effectively solved. Therefore, the main computational cost of the implicit scheme is the correction of the growth rate.

The profile $n(r,t)$ is discretised on a grid, where the continuous radial position is replaced by a discrete index i and the profile is represented by $n_i(t)$. The linearisation of the correction step (A.2) around $n_i(t + \delta t) = m_i$ follows as

$$\left[\left(1 + \frac{\delta t}{2}\gamma_i[m]\right)\delta_{ij} - \frac{\delta t}{2}m_i\frac{\partial\gamma_i}{\partial n_j}\Big|_m\right]n_j\left(t + \delta t\right) =$$
$$= n_i(t) + \frac{\delta t}{2}\gamma_i\left[n(t)\right]n_i(t) - \frac{\delta t}{2}m_j\frac{\partial\gamma_i}{\partial n_j}\Big|_m m_j \tag{A.3}$$

where we use a repeated index summation over j but not over i. This is an equation for every radial position i, with coupling to other terms due to $\partial\gamma_i/\partial n_j|_m$. This equation needs to be modified at the end points to satisfy the boundary condition. The boundary conditions used were an absorbing wall at $r = a$, i.e $n(r = a) = 0$ and a Neumann boundary condition of the form $\partial n/\partial r = 0$ at the center to respect the symmetry.

The implicit time propagation was implemented for two different scenarios. Firstly, radiative theory without radial gradients in the electric field, diffusion constant or background plasma parameters, which was used in section 5.2.1. Secondly, for the non-radiative theory with gradients in the electric field, but still no gradients in the diffusion coefficient or the plasma parameters, which was used in section 5.2.2. For both of these cases the definition of k^2 in equation (5.6) reduces to

$$k^2 = -n^{-1}\frac{1}{r}\frac{\partial}{\partial r}r\frac{\partial n}{\partial r} \approx -\frac{1}{r_i}\frac{n_{i+1} - n_{i-1}}{2\delta r n_i} - \frac{n_{i+1} - 2n_i + n_{i-1}}{n_i\left(\delta r\right)^2} \tag{A.4}$$

and therefore $\partial k_i^2/\partial n_j$ forms a tridiagonal matrix as

$$\frac{\partial k_i^2}{\partial n_j} = -\frac{1}{n_i}\left[\frac{\delta r + 2r_i}{2r_i\left(\delta r\right)^2}\delta_{i+1\,j} + \left(k_i^2 - \frac{2}{\left(\delta r\right)^2}\right)\delta_{ij} - \frac{\delta r - 2r_i}{2r_i\left(\delta r\right)^2}\delta_{i-1\,j}\right]. \tag{A.5}$$

The last piece to form the equation system (A.3) is to calculate $\partial\gamma_i/\partial k_j^2$ to use with the chain rule together with (A.5). As the growth rate correction is only dependent on k^2, $\partial\gamma_i/\partial k_j^2$ is a diagonal matrix. The diagonal is formed by differentiating the integral equation (3.21) which results in

$$\frac{\tau}{E-1}\frac{\partial\gamma}{\partial k^2} = -\frac{1}{k^2}\frac{\int_{p_*}^{\infty}dq\,e^{-\int_{p_*}^{q}dq'\,x+\alpha(p(q'))}\left(\int_{p_*}^{q}dq'\,\alpha(p(q'))\right)}{\int_{p_*}^{\infty}dq\,e^{-\int_{p_*}^{q}dq'\,x+\alpha(p(q'))}\left(q - p_*\right)}$$
$$= \frac{1}{k^2}\frac{\int_0^1 d\lambda\,\mathcal{G}(q)\left[\ln(\mathcal{G}(q)) - \alpha(p_{\max})(q - p_*)\right]}{\int_0^1 d\lambda\,\mathcal{G}(q)\left(q - p_*\right)} \tag{A.6}$$

and in the second line the notation has transitioned to the one used in section 4.1, where $q = p_* - \Gamma^{-1}\ln\lambda$, $\Gamma = x + \alpha(p_{\max})$ and $\mathcal{G}$ is defined by equation (4.2). The second form is more suitable for the numerical implementation as it can re-use the $\mathcal{G}$ from the numerical solver for the growth rate. In fact, $\mathcal{G}$ only needs to be constructed once for every radial position as for a changing k^2 it need only be re-scaled based on the definition (4.2).

A.2 Validation PDE - solver

For the validation in 5.2.2 we use a PDE-solver for equation (3.4), which is the PDE from which the integral formulation (3.7) of the growth rate originates. Equation (3.4) is formulated in terms of the coordinates t, r, p, but we will use a normalised radial position $x = r/a$ and a momentum coordinate $\lambda = \exp\left(-\Gamma(p - p_*)\right)$ where Γ is a free parameter. In these coordinates equation (3.4) takes the form,

$$\frac{\partial F}{\partial t} - \Gamma\frac{E-1}{\tau}\lambda\frac{\partial F}{\partial \lambda} = \frac{1}{x}\frac{\partial}{\partial x}x\nu_d\frac{\partial F}{\partial x} \tag{A.7}$$

where $\nu_d = D/a^2$. In these coordinates the radial and momentum dimension both extend between $[0, 1]$.

An equidistant grid in all three coordinates is introduced according to $x_i = \Delta x \cdot i$, $\lambda_j = \Delta\lambda \cdot j$ and $t_n = \Delta t \cdot n$, on which the distribution function is discretised $F(x_i, \lambda_j, t_n) = F_{i,j}^n$, where Δx, $\Delta\lambda$ and Δt are the discretisation lengths in the three directions. To have an implicit scheme the spatial and momentum derivatives are taken to be the average of those in the current time step n and the following one $n + 1$. For the diffusion operator this corresponds to a Crank-Nicolson scheme [88], but the introduction of an implicit method in the momentum coordinate breaks the tridiagonality of the equation system to be solved. A finite difference scheme based on centre derivatives result in

$$(1 + a_{ij})F_{i,j}^{n+1} - b_{ij}^+ F_{i+1,j}^{n+1} - b_{ij}^- F_{i-1,j}^{n+1} - c_i\lambda_j F_{i,j+1}^{n+1} + c_i\lambda_j F_{i,j-1}^{n+1} =$$
$$= (1 - a_{ij})F_{i,j}^n + b_{ij}^+ F_{i+1,j}^n + b_{ij}^- F_{i-1,j}^n + c_i\lambda_j F_{i,j+1}^n - c_i\lambda_j F_{i,j-1}^n \tag{A.8}$$

with

$$\begin{aligned}
a_{ij} &= (\nu_d)_{i,j}\frac{\Delta t}{(\Delta x)^2} \\
b_{ij}^+ &= \frac{\Delta t}{2(\Delta x)^2}\left(\left(1 + \frac{\Delta x}{2x_i}\right)(\nu_d)_{i,j} + \frac{(\nu_d)_{i+1,j} - (\nu_d)_{i-1,j}}{4}\right) \\
b_{ij}^- &= \frac{\Delta t}{2(\Delta x)^2}\left(\left(1 - \frac{\Delta x}{2x_i}\right)(\nu_d)_{i,j} - \frac{(\nu_d)_{i+1,j} - (\nu_d)_{i-1,j}}{4}\right) \\
c_i &= \frac{\Delta t}{4\Delta\lambda}\frac{E_i - 1}{\tau_i}\Gamma
\end{aligned} \tag{A.9}$$

and $(\nu_d)_{i,j} = \nu_d(r_i, \lambda_j)$, which is a linear system of equations for the distribution function in the following time step. These equations need to be joined with the boundary conditions, which for the radial directions are $F_{\max,j}^n = 0$ and $F_{0,j}^n = F_{1,j}^n$. In momentum space we assume there to be no particles at infinite energies, $F_{i,0}^n = 0$, and the integral boundary condition (3.7) for the distribution function at p_* is discretised by a trapezoid rule and written in terms of a matrix multiplication as
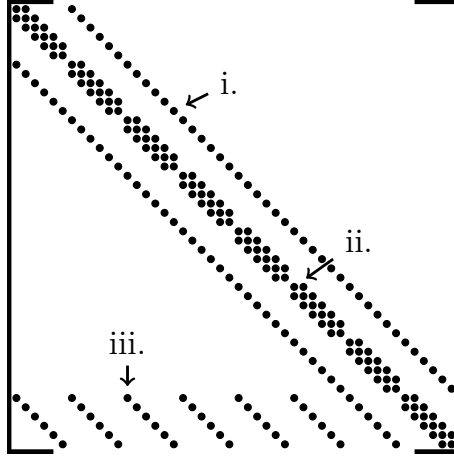
Figure A.1: Illustration of the non-zero entries for the system of equations which form the left hand side of equation (A.8) when 6 inner radial points and 8 inner momentum points have been used. $F_{i,j}^{n+1}$ is made into a vector by putting all radial points for a given momentum next to one another in chunks, which are then put after one an other. i. Corresponds to the connection in momentum-space, and is far off diagonal due to the ordering of $F_{i,j}^{n+1}$. ii. The radial connection, the periodic diamond shape is an effect of the radial boundary condition. iii. Corresponds to an integral over momentum-space for all radial positions and is due to the boundary condition in $F(p_*)$.

$$F_{i,\max}^{n} = \frac{\gamma_r \tau}{\Gamma_g \left(E - 1 - \frac{d\lambda \gamma_r \tau}{2\lambda_{\max}} \right)} \left(d\lambda \left[\frac{1}{2\lambda_2}, \frac{1}{\lambda_3}, \ldots, \frac{1}{\lambda_{\max-1}} \right] \begin{bmatrix} F(\lambda_2) \\ F(\lambda_3) \\ \vdots \\ F(\lambda_{\max-1}) \end{bmatrix} \right) \quad (A.10)$$

which for every time step is incorporated partly explicit and partly implicit into the $j = \max$ equation of (A.8).

By restructuring $F_{i,j}^{n+1}$ for a given n to be a vector and using the boundary condition, the left hand side of equation (A.8) can be written as a constant matrix multiplied by F. The constant matrix is illustrated in figure A.1. As the matrix is constant it can be inverted once, and re-used in the following time steps. The matrix in figure A.1 is sparse, but its inverse is not. Therefore, in this case it is actually more efficient to LU-factorise the matrix and solve the upper- and lower- triangular equation systems, which are sparse, in every time step then multiply with a dense inverse.